Particle and Bacteria Sorting in Viscoelastic Fluids Using an Elasto-Inertia-Magnetic Fractionation Method

Seyed Sina Dibaji

A THESIS SUBMITTED TO

THE FACULTY OF GRADUATE STUDIES

IN PARTIAL FULFILLMENT OF THE REQUIREMENTS

FOR THE DEGREE OF

MASTER OF APPLIED SCIENCE

Graduate Program in

MECHANICAL ENGINEERING

York University

Toronto, Ontario

February 2019

Abstract

Detection of harmful biological substances in food at the Point of Use (PoU) is very important for the prevention of foodborne diseases. Sample and reagent preparation at the PoU, as a necessary step before detection, is urgently needed. Portable and field-deployable sample preparation microfluidic devices for manipulating particles and biological substances in water have been widely studied. During the recent years, more attention has been given to particles separation in non-Newtonian fluids due to their rheological similarity to the prominent fluids such as food (e.g. milk) and bodily fluids (e.g. blood). However, the mechanism of particle focusing and separation in non-Newtonian fluids is less understood, mainly due to the dominance of elastic forces in such flows. Accordingly, we developed a microfluidic device to investigate the effect of elastic, inertial, and magnetic forces on the focusing of magnetic (9 and 15 μm) and non-magnetic (15 μm) particles in synthetic viscoelastic fluids with various viscosities. The device included a square microchannel with a side permanent magnet, expanding symmetrically downstream to a wider channel to drop the particles velocity for on-chip imaging. We investigated the effect of multiple parameters on the focusing of each particle experimentally and analytically, in order to obtain physical understanding and the best recipe in which multiplex particle or bacteria separation could be achieved with high efficiency. The studied parameters included the microchannel cross-sectional size, flow rate, fluid viscoelasticity, and magnetic field strength and exposure time. We then used the results of the parametric study to perform Triplex-Inertia-Magneto-Elastic (TIME) sorting of magnetic and non-magnetic particles with >92% purity and efficiency. To demonstrate the potential use of this method in biological applications, we immunologically conjugated two types of bacteria to magnetic and non-magnetic particles and separated them from each other in the microfluidic device with a purity and efficiency of >99%. This study provides the foundation for development of devices for separation of bio-substances in viscoelastic fluids, immunologically attached to microparticles. Our device has the potential to be used for on-site sample preparation along with a variety of biosensors to render biodetection possible at the PoU.

Acknowledgement

I would like to start by thanking my supervisor, Dr. Pouya Rezai for giving me the opportunity to take this project at the ACµTE lab and for his continuous guidance and support during this time. One major thing that I have learnt from Dr. Rezai is to always aim for better, always try to reach higher, and never submit to the tendency for inertia. This is the lesson that I tried to keep in my mind during my research at ACµTE lab and will never forget in my future career and life. I will always be grateful to him.

I would also like to thank Dr. Siu Ning Leung and Dr. Gerd Grau for accepting to join my defence committee and examine my thesis.

I would like to express my sincere gratitude and love to my wonderful parents, Mina and Rasoul, my smart and beautiful sister, Mahsa, and the love of my life, my beloved Zahra whose continuous and unconditional love and support was the drive for me to go on. This thesis would not be finished without them. I am also thankful to my dear friends in USA, Iran and Canada who were always there for me in happiness and sadness, despite the miles and borders between us. Thank you, Cyrus, Matin, Arash, Bahar, Arman, Zahra, and Hamid.

There have been ups and downs, good days and bad days, and sweet and bitter memories in the past 29 months but I always believed that it all has been a process for eventually reaching success, happiness and prosperity and one should always stay hopeful and try for the best. As the great Persian poet, Hafez said:

If, for a space of two days, to our desire, the sphere's revolutions turned not,

Ever, in one way, the state of revolution is not, suffer not grief.

Although the stage of this world is very fearsome, and the purpose hidden,
There is not a road, whereof is no end, suffer not grief.

Table of Contents

Table of Figures

Chapter 1

INTRODUCTION AND LITERATURE REVIEW

1.1 INTRODUCTION AND MOTIVATION

One of the research topics under extensive investigation globally over the past few decades is controlling the fatal diseases in remote communities and developing countries with limited access to advanced healthcare systems and technologies[1–3]. One of the main reasons behind the prevalence of life-threatening diseases in these places is the food and water contamination and lack of access to proper monitoring systems[4]. Suspended analytes such as pathogenic bacteria in water and food can easily spread to large volumes and cause health issues to large bodies of people within a relatively short period of time. Naturally, there are multiple types of microscopic analytes present at high concentration in our food, however, the pathogenic microbes, which usually have much lower concentration, even down to an order of one cell per milliliter, are the ones that should constantly be monitored, detected and eradicated. There should be rapid and sensitive technologies available to detect microbial contaminants at the point-of-(food and water)-use, with low cost and

without expensive and labor-intensive lab equipment[5–8]. This challenge is more prevalent in resource-limited communities and developing countries where modern water purification and food sterilization systems are inaccessible.

Samples obtained directly from nature (e.g. ground water), aqueous foods (e.g. raw milk), and bodily fluids (e.g. blood) are relatively complex fluids, containing a high variety of suspended and dissolved analytes such as particles, cells, parasites, bacteria, viruses, proteins, and minerals[9]. The microbial contaminants in food and water have sizes in the range of nanometers (e.g. viruses) to micrometers (e.g. bacteria). They are very difficult to detect since they are outnumbered by the other suspended matter in the liquid sample[10]. Accordingly, one of the most challenging and time-consuming steps in microbial detection is the sample preparation process wherein the target microbes should be labeled and separated from the rest of the content that can cause problems such as false positives and inhibition during the detection process[11]. As mentioned earlier, sample preparation and microbial detection is preferred to be conducted at the points of sample acquisition, so that corrective actions to prevent pathogen outbreaks can be rapidly undertaken.

The current techniques that are used for testing food and water are not usually portable and applicable in low-resource areas due to their relatively high cost and being time consuming. These methods often require collecting the samples, storage and transportation to central screening labs, sample preparation, and analysis. Sample preparation usually requires a series of equipment including but not limited to centrifuge, filters, incubators and so on to sort and separate target analyses from non-targets. Cellular or molecular analysis techniques such as cell cytometry, ELISA[*], and PCR[†] are also labor-, time- and equipment-intensive and not suitable in their

[*] Enzyme-linked immunosorbent assay (ELISA) is a common plate-based assay method for detecting biological substances such as antibodies and proteins.

[†] Polymerase chain reaction (PCR) is method commonly used for making copies of (amplifying) a DNA sequence.

conventional forms for Point-of-Use (PoU) detection. Accordingly, there is a need for portable devices that can carry out sample preparation and analysis with a relatively low cost and ease of use, where the operator does not require significant professional expertise in the field of biological testing.

The need for performing biological testing and screening at the point of sample acquisition or PoU using portable devices has accelerated the movement towards miniaturization of electromechanical systems for fluid handling and analyte detection in recent years[2,5]. Based on this trend, various microfluidic PoU detection and diagnosis devices have gained extensive attention from researchers for various applications[6,12–14]. The main purpose of these devices is to become commercially available and applicable where there is a need for rapid and low-cost detection of harmful substances in fluids, such as in low-resource areas or on the field of sample acquisition. However, in most of these devices, the sample preparation process usually takes place off the chip and the target analyte separated from the rest of micro-nano-particles is inserted into the device for detection[14,15]. This decreases the usability of the device in certain PoU applications where off-chip sample preparation is not achievable, mostly due to a lack of access to equipment and professional labor. As such, there is a need for the development of portable and field-deployable sample preparation devices that can be integrated with biosensors for full deployment of microfluidic PoU diagnosis and detection technologies.

Micro- and nano-particle separation, as a major step in sample preparation, can be done at the PoU with microfluidic devices[16–18]. The need for microfluidic microparticle separation, especially at the point of fluidic sample acquisition, is present in many applications such as cell[17,19–22] and bacteria[23–26] separation for biotechnology, biomedical assays and food monitoring. Cells and bacteria can either act directly as target microparticles[27–30], be conjugated with magnetic and non-

magnetic particles as carriers[26,31–33], or be labeled with particles to achieve properties they do not possess such as larger size and/or magnetic characteristics. The tagging usually happens using micro- or nano-particles coated with antibodies that have an affinity towards the antigens of the target cells or bacteria[34]. Below, we review various microfluidic techniques that have been reported for particle separation and their applications in the above-mentioned fields.

1.2 MICROFLUIDIC PARTICLE SORTING METHODS

Microfluidic particle separation methods can be categorized into two groups based on their separation mechanisms and the forces exerted on the particles. If particles separate from each other solely due to the hydrodynamic forces applied from the fluid flow, the technique is called a "Passive Sorting Method". In cases where there is an external source of energy (other than the pump that moves the fluid) and external forces are exerted on the particles, the technique is called an "Active Sorting Method". In the next two sections, we will review the passive and active sorting methods with their applications in particle separation in Newtonian fluids.

1.2.1 Passive Microfluidic Particle Sorting Methods

Drag and inertial forces exerted from the fluid to the particles and the laminar hydrodynamics of the flow can be used to separate particles from each other in passive microfluidic devices. One of the main characteristics affecting the magnitude of these forces is the particle size. Hence, microfluidic devices have been developed to sort particles based on their hydraulic diameters. Among these passive sorting methods, deterministic lateral displacement (DLD)[35], pinched flow

fractionation (PFF)[36], and inertial microfluidics[37,38] in straight[39–41] and spiral[42,43] microchannels can be named.

DLD was first developed in 2004 by Huang et al.[35]. As shown in Fig. 1-1a, this method uses an array of small pillars in a channel to separate the particles based on their sizes. DLD works because around each pillar, the smaller particles remain in the same streamline while the larger particles enter a new streamline due to the force exerted on them from the pillar (F_{DLD}) and thus become separated from the smaller particles[44]. In Fig. 1-1a, the size and configuration of pillars and their arrangement direction inside the channel help moving all the large particles to the right and all the small particles to the left-hand side of the channel. DLD microdevices can be modified to separate multiple particles by using a series of different pillar arrays to separate different particles from the stream, one at a time (Fig. 1-1b)[45]. Among the applications of this method, separating blood cells (red, white, and platelets) from the plasma is the most common[44,45]. This method can be disadvantageous due to its relatively low-throughput and frequent blockage by particle clogging in between the pillars.

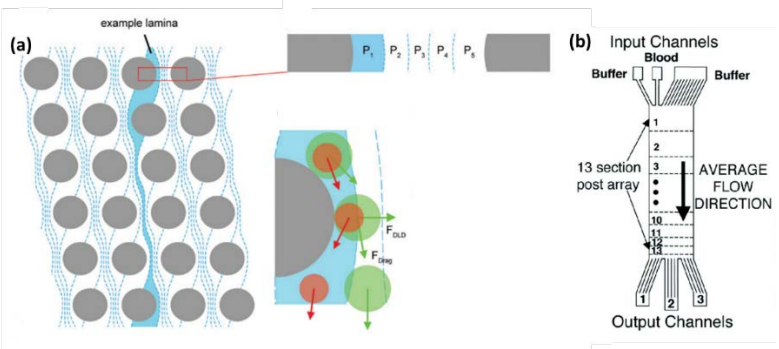

Figure 1-1(a) Deterministic Lateral Displacement (DLD) separation method using an array of micropillars in a microchannel. Larger particles are separated from the smaller particles and move to another streamline due to the force exerted from the pillar[46]. (b) Using a series of pillars with different configurations to separate multiple particles or cells from each other[45]. Permissions obtained from RSC.

PFF was also introduced in 2004 by Yamada et al.[36]. As shown in Fig. 1-2a, PFF devices have two inlets with different flow rates, a pinched section with a small cross-section, and an expansion

zone. They can separate two particles based on their size (Fig. 1-2a insert). The upper inlet containing the particle solution has a lower flow rate than the lower inlet containing the sheath flow. In the pinched section, particles with different sizes take position at different streamlines with the aid of the sheath flow and become separated at the downstream expansion zone. Vig and Kristensen[47] have attempted to enhance the performance and separation efficiency of the PFF method by adding an additional segment in the expansion zone, which expands the part of the flow in which the two particle streams are present. A major drawback of this method is the need for the sheath flow which dilutes the solution and requires higher control on the flow rates using equipment such as additional syringe pumps.

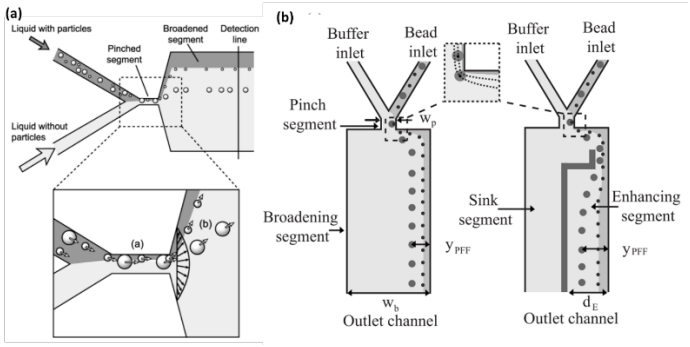

Figure 1-2 (a) Pinched Flow Fractionation (PFF) method using a pinched section to separate particles based on their size[36]. (b) Modifying the PFF channel to enhance the separation efficiency[47]. Permissions obtained from ACS and AIP.

Many researchers have exploited the size-dependent forces on the particles to focus and separate them in straight and spiral channels. In Newtonian flows where the size of the particle, a, is considerably large in accordance to the hydraulic dimeter of the channel, D_h, the inertial forces can help focus the particles (with $\frac{a}{D_h} > 0.07$) at single or multiple equilibrium positions depending on the flow condition and the channel geometry[48]. This area of research is called inertial separation or inertial microfluidics[38,49,50].

Inertial separation in straight channels can happen in various device designs which will be discussed among a few examples. Generally, all these devices implement the difference between

the magnitude of inertial forces for particles with different sizes. This method works since the particles tend to focus at the centers of the long walls in a rectangular microchannel, due to the balance between the shear- and wall-induced inertial lift forces as shown in Fig. 1-3a and described further in Chapter 2. Focusing happens faster for larger particles since the magnitude of the above forces depend on the size of the particle. Particle separation can be achieved by controlling the aspect ratio (i.e. height/width) of the channel and the flow rate. Inertial separation offers simple design using straight microchannels, a high throughput, and no need for a sheath buffer flow. However, its performance is limited to separating two particles at a time. Multiple separation steps are needed to separate more than two particles based on their sizes.

Zhou et al.[39] introduced an inertial microfluidic separation device (Fig. 1-3b) in which particles first focus at the center of the longer walls in a high-aspect-ratio channel (H>W). This channel then expands into a low-aspect-ratio channel where the larger particles migrate faster to the center and separate from the smaller particles. Wang et al.[40] implemented the same idea but with modifications to make it easier to fabricate the device, due to difficulties associated with making high-aspect-ratio channels (Fig. 1-3c). In their device, particles first focus at the center of the longer wall in a low-aspect-ratio channel. This channel then bifurcated into two low-aspect-ratio channels in which the larger particles migrate faster to the center of the channel and get separated from the smaller ones. Wang and Papautsky[41] developed a device to perform separation in multiple steps and achieve multiplex separation (Fig. 1-3d). In this method, particles focus at the center of the long walls in a high-aspect-ratio channel. The larger particle can be separated from the stream by placing an expansion and contraction vortex generator section beside the channel. This was done twice to separate three particles from each other as shown in Fig. 1-3d.

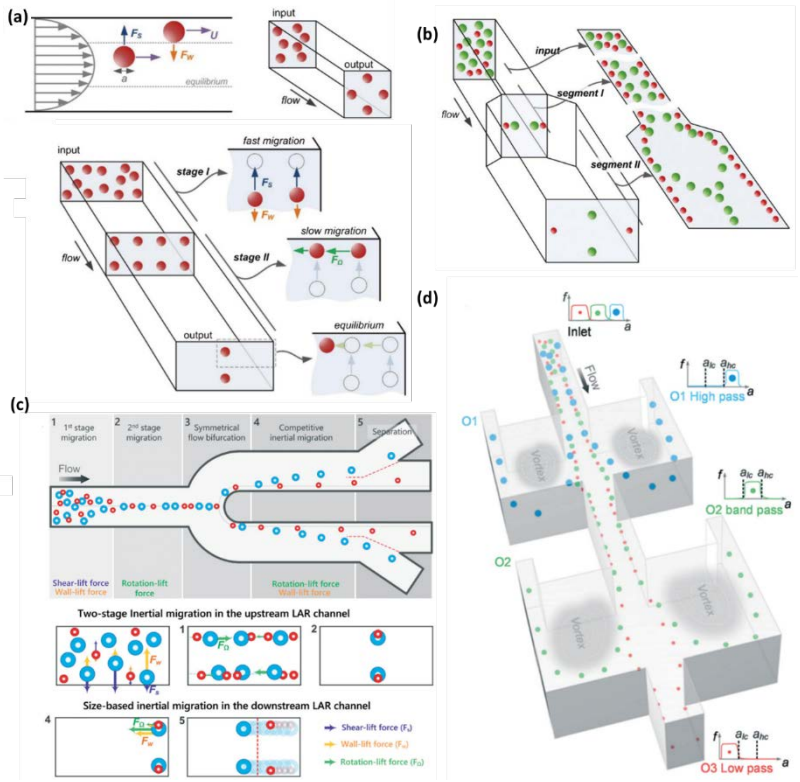

Figure 1-3 (a) Inertial particle focusing in a rectangular microchannel under the effect of shear-induced (F_s) and wall-induced (F_w) inertial forces[51]*. (b) Separation of particles based on their size by changing the aspect ratio of the channel*[39]*. (c) Separation of particles based on their size by bifurcating the channel*[40]*. (d) Multiplex separation of particles based on their size with multiple separation steps and vortex sections beside the channel*[41]*. Permissions obtained from RSC.*

As discussed above, inertial separation of more than two particles based on their size is not achievable in one step using straight microchannels. In these cases, inertial separation in spiral channels has been used to achieve sorting of up to four particles inertially[52]. Separation in these devices (Fig. 1-4) happens due to the balance of inertial lift (F_L) and Dean drag (F_D) forces on the particles which can be controlled by changing the flow rate, fluid properties, and the radius of curvature and number of loops in the spiral channel. In a spiral channel, multiple counter-rotating vortex flows (Dean flow) are generated due to a pressure mismatch between the inner and outer walls of the channel. The Dean flow drags the particles laterally and circulates them three-dimensionally in a spiral channel[49,53]. The presence of the aforementioned inertial force, if dominating the Dean drag force, leads to focusing of particles at the inner wall of the channel, with the focusing location highly dependent on the particle size[42,43].

Bhagat et al.[42] first introduced a microfluidic device with spiral channels to separate two particles based on their size (Fig. 1-4a). At the end of the channel, larger particles (7.32 μm) focus near the inner wall under the influence of inertial lift force while the smaller particles (1.9 μm) are moved towards the outer wall due to the dominant effect of the Dean drag force. Continuing on this work, the same group later showed that larger particles with different sizes can reach different equilibrium positions near the inner wall of the channel due to different ratios of inertial lift and Dean drag forces (Fig. 1-4b)[43]. Therefore, they could achieve triplex separation of 10, 15, and 20 μm particles in their device. Another technique which can separate up to four particles based on their size using a spiral channel was introduced by Sarkar et al. (Fig. 1-4c)[52]. In this device, particle separation happens with the help of a sheath flow. Larger particles (6 and 10 μm) focus near the inner wall and smaller particles (1 and 4.5 μm) focus near the outer wall. They used this method to separate rare proteins and cells from blood by performing affinity-based binding to particles and using particles as size-coded carriers for the analytes. However, this technique often requires a high volumetric flow of sheath fluid, its design is more complicated than straight channels, and its operation is restricted by the channel's geometry (radius and number of spiral loops).

1.2.2 Active Microfluidic Particle Sorting Methods

Most of the existing passive sorting methods can only separate particles based on their sizes and are unable to distinguish particles with the same size but different intrinsic characteristics such as magnetic, dielectric, or optical properties. To address this limitation and to increase the control over manipulation of particles and cells, an external force can be applied in a microfluidic device. These active and semi-active sorting methods may implement dielectrophoresis[54], acoustics[55], optics[56], and magnetophoresis[19,24,31,57–64] transduction modalities. Among these methods, magnetic

separation is one of the most favorable ones due to the fact that it does not require an outside source of energy due to the use of permanent magnets, which enhances the simplicity and portability of the device for PoU applications. Additionally, magnetic micro- and nano-particles have been widely used and commercialized as immunological labels for various cells and molecules[5,65].

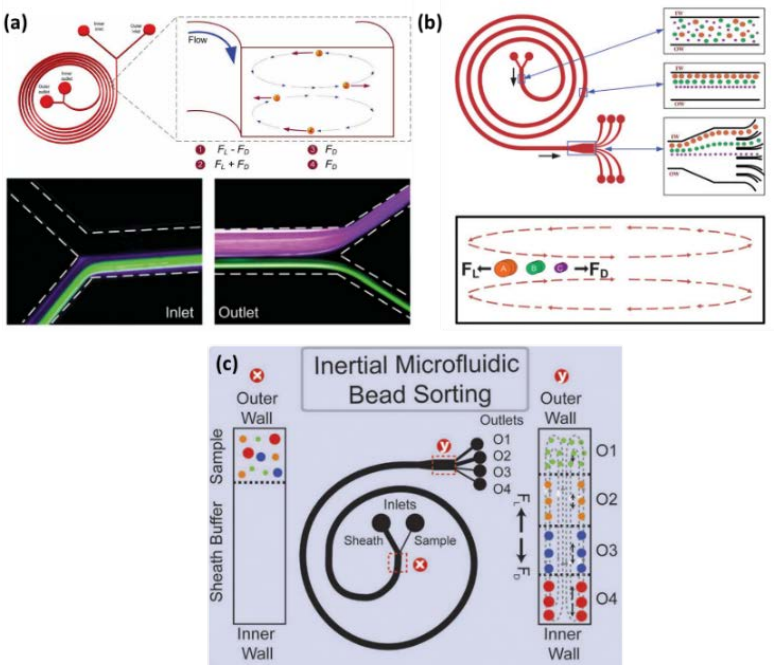

Figure 1-4 (a) Particle separation in spiral channels under the effect of Dean drag (F_D) and inertial lift (F_L) force. Larger particles focus near the inner wall due to the balance of F_D and F_L. Smaller particles keep moving with the Dean flow and can be separated from the larger particles[42]. (b) Triplex separation in spiral channels. Particles acquire different equilibrium positions near the inner wall due to the difference in the ratio of Dean drag force and inertial lift force.[43] (c) Separation of four particles based on their size, by combining the focusing of larger particles and flow of smaller particles[52]. Permissions obtained from RSC.

Macroscale separation of magnetic and non-magnetic beads using high gradient magnetic fields was first shown by Miltenyi et al. in 1990 (Fig. 1-5)[66]. In their technique which is called Magnetic Activated Cell Sorting (MACS), magnetically-tagged cells and non-tagged cells flow down a tube surrounded by a high gradient magnet (HGM) column, where the magnetic cells remain in the tube while the non-magnetic cells flow through the column. The magnetically-tagged cells will then be released and recovered by removing the magnet.

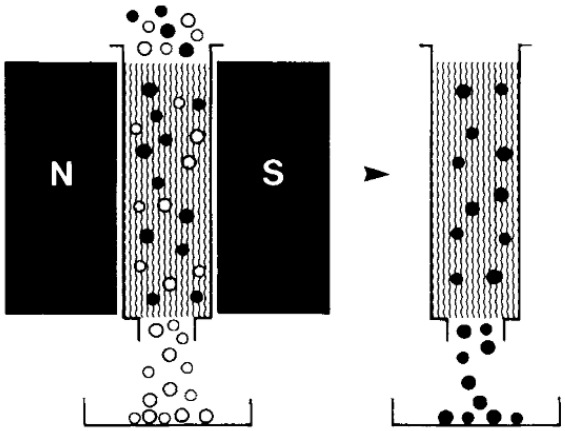

Figure 1-5 Magnetic Activated Cell Sorting(MACS) method, consisting of a tube surrounded by a high gradient magnet column to separate magnetic cells from non-magnetic ones[66]. Permissions obtained from John Wiley and sons.

Different methods have been developed by researchers to perform microfluidic magnetic separation and among those, we can name on-chip free flow magnetophoresis[61], H-shaped magnetic separator[64], and multitarget magnetic activated cell sorter (MT-MACS)[58].

On-chip free flow magnetophoresis was developed by Pamme and Manz in 2004[61]. In this method, a laminar stream of sample solution enters the separation chamber, along with multiple laminar streams of a buffer. In the separation chamber, magnetic particles deflect from their stream toward a magnet beside the channel. The amount of deflection differs for magnetic particles with different sizes. The non-magnetic particles continue in the same stream as they enter the chamber. Separation of two magnetic particles from a non-magnetic particle has been reported using this device (Fig. 1-6). Dr. Pamme and her group later published several papers on the development and applications of this method in cell detection and separation[24,60,67–69].

H-shaped magnetic separation devices offer simple design for separating magnetic and non-magnetic particles in the presence of a buffer flow. These devices consist of two inlets and two outlets and usually require a sheath flow to operate (Fig. 1-7). Particles enter from one of the inlets while the other inlet contains the buffer flow. The magnet deflects the magnetic particles, changing their streamlines towards one of the outlets, while the non-magnetic particles (or in some cases

small magnetic particle) stay in the same streamline and exit from the other outlet. Two configurations can be used for these devices where the magnet can either be located at the sides of the H channel (Fig. 1-7a)[70] or beside the middle channel (Fig. 1-7b)[64]. It should be noted that these devices should not necessarily have 90° angle channels and any device that works based on the same principal is considered an H-shaped magnetic separation device.

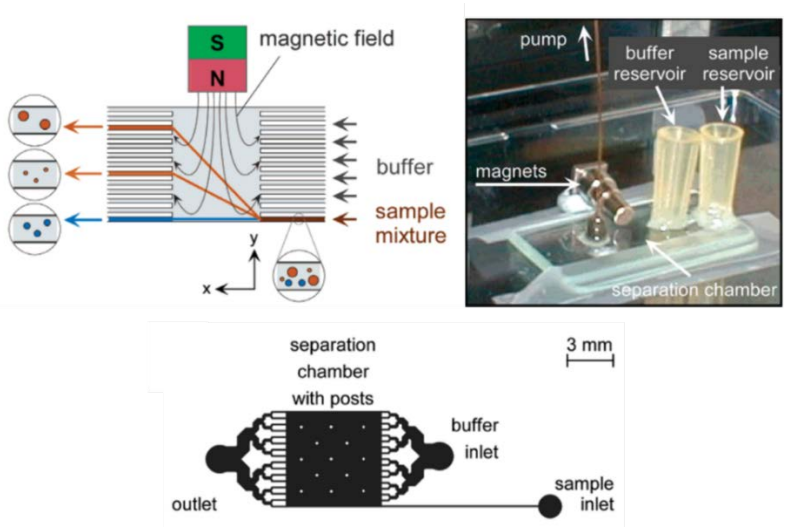

Figure 1-6 On-chip Free Flow Magnetophoresis method schematic, actual device and design[61]. Permissions obtained from ACS..

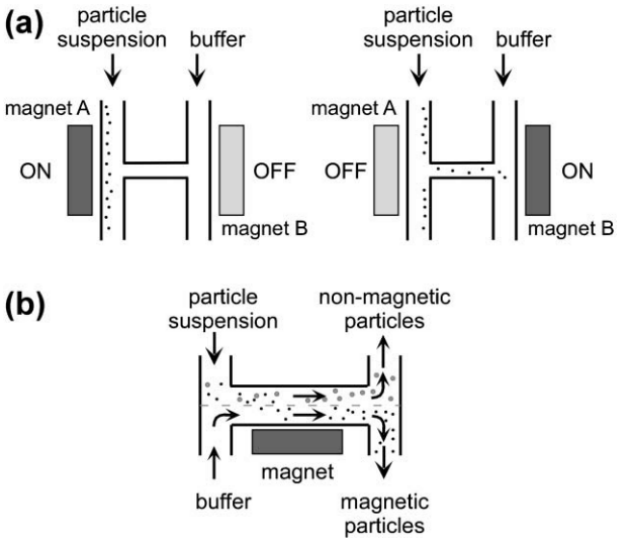

Figure 1-7 Different configurations of H-shaped magnetic separation devices with (a) magnet on either side of the H and (b) magnet beside the middle of the H.[62] Permissions obtained from RSC.

Multitarget Magnetic Activated Cell Sorter (MACS) was introduced by Adams et al. in 2008 (Fig. 1-8)[58]. This device consists of two inlets for the particle and buffer solutions and three outlets for extracting the magnetic particles and the waste solutions. Right before the first two outlets, microfabricated ferromagnetic stripes (MFS) were used to generate local magnetic field gradients to guide a specific particle with a certain size toward the outlet (Fig. 1-8a). The first MFS was designed with a high angle to deflect the larger magnetic particles, while the second MFS with a lower angle could deflect the smaller magnetic particles. Non-magnetic particles stayed in the same streamline and exited from the third outlet (Fig. 1-8b). They implemented this method for separating biotargets by affinity-binding them to the magnetic particles. Non-target non-magnetic cells acted as the non-magnetic particles.

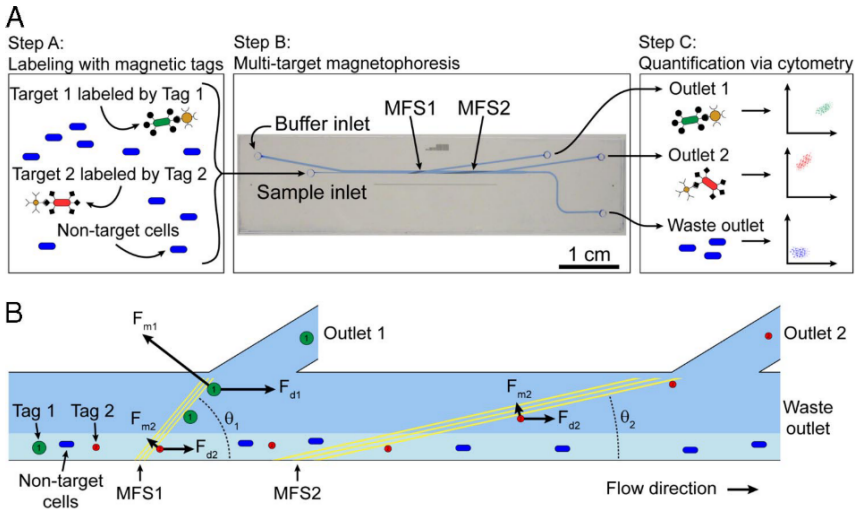

Figure 1-8 Multitarget Magnetic Activated Cell Sorter (MACS) capable of separating two magnetic particles with different sizes from non-magnetic particles using microfabricated ferromagnetic stripes (MFS)[58].

The passive sorting methods discussed in the previous section can be combined with the active techniques to create hybrid separation approaches with improved performances in terms of multiplexing and separation efficiency. Recently, a separation device based on multiplex inertia-magnetic fractionation (MIMF) was developed by our group to sort magnetic and non-magnetic particles in water[71,72]. This device consisted of a straight rectangular microchannel with a

permanent magnet beside it, followed by an expansion zone (Fig. 1-9a). In this high-throughput and sheathless device, 5, 11, 15 µm magnetic and 35 µm non-magnetic particles were inertially focused in a rectangular straight channel and separated from each other at an expansion zone based on their size, due to the use of the permanent magnet beside the channel. The magnitudes of inertial and magnetic forces which depend on the size of particles align them in different equilibrium positions which leads to their separation at the expansion zone (Fig. 1-9b).

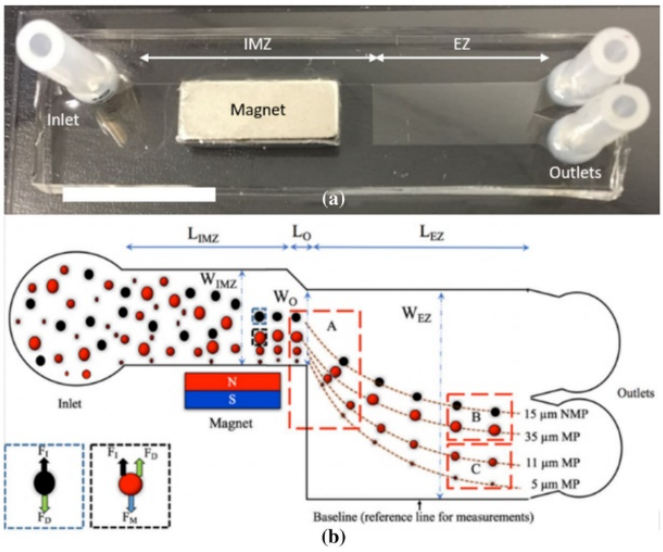

Figure 1-9 Multiplex Inertio-Magnetic Fractionation (MIMF) method for separation of three magnetic particles from a non-magnetic particle. Particles attain different equilibrium positions due to the balance between inertial lift, drag, and magnetic forces. (a) actual device. (b) schematic of particle separation.[71] Permissions obtained from Springer Nature.

Non-magnetic microparticles and cells can also be magnetically manipulated and sorted in ferrofluids[73–75]. Ferrofluid is a term used for stable and uniform suspensions of magnetic nanoparticles in fluids like water. Ferrofluids are highly magnetizable and can be used for transportation of diamagnetic particles in the presence of a magnetic field[21,62]. The ferrofluid-based microfluidic devices work based on the principle that non-magnetic particles get repelled from the magnet due to the difference between the magnetic susceptibility of the particle and the ferrofluid. Zhu et al.[74] demonstrated the separation of two non-magnetic particles (1 and 9.9 µm, 1.9 and 9.9 µm, and 3.1 and 9.9 µm) in an H-shaped device (Fig. 1-10a). Particles in the ferrofluid enter the

device from one of the inlets and ferrofluid buffer enters from the other inlet. The magnet beside the middle channel repels the particles. The force on the larger particles is higher and it deflects the particles into the sheath flow to exit from the upper outlet, while the smaller particles stay in the same stream and exit from the lower outlet. As a biological application, Zhu et al. used the same technique to separate *E. coli* bacteria from Yeast cells[28]. They first used 1 and 7.3 µm particles to characterize the separation performance of their device and then substituted the particles with the biological analytes with similar sizes, i.e. *E. coli* and Yeast cells. In another work, Zeng et al.[75] showed the separation of 3 and 10 µm non-magnetic particles in a ferrofluid using a straight channel and two offset magnets (Fig. 1-10b). In this device, a ferrofluid spiked with two particles enters the channel from a single inlet. At the beginning of the channel, both particles will be repelled to one side of the channel using a strong magnetic field at one side of the channel. Another magnet is placed farther at the opposite side of the channel which generates a weaker magnetic field. As a result, larger particles get repelled faster than the smaller ones and get separated at the outlet.

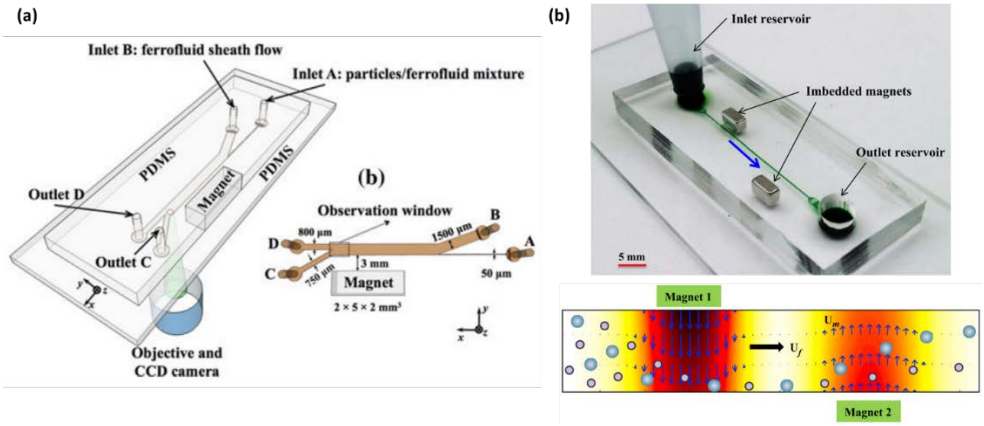

Figure 1-10 Ferrofluid-based particle separation devices (a) using an H-shaped device with a buffer flow to deflect the larger particles into the upper outlet[74] and (b) using two offset magnets to separate particles based on their size sequentially[75]. Permissions obtained from Springer Nature and Elsevier.

Most of the techniques discussed above have been developed using water as the carrier fluid. However, in many of the applications in biotechnology and food testing, the carrier fluid is a non-

Newtonian fluid such as blood, DNA solutions and milk. In a non-Newtonian fluids, the viscosity of the fluid changes with respect to the flow velocity gradient, which can introduce new forces on the particles. In the next section, we will discuss how the aforementioned techniques can be modified to also be applicable for using with viscoelastic fluids and how using a viscoelastic fluid as a carrier fluid can sometimes enhance the separation performance.

1.2.3 Particle Sorting in Viscoelastic Fluids using Microfluidics

Many of the biological fluids such as blood, saliva, milk and DNA solutions are known to exhibit viscoelastic behavior due to the abundance of deformable cells or ling molecular chains in their complex structure[76]. Being viscoelastic means that the shear stress inside the fluid does not change linearly with the deformation rate, a behavior that is not expected from a Newtonian fluid like water. As it turns out, non-Newtonian properties and the behavior of fluids (e.g. shear-thinning or shear-thickening) play a major role in particle focusing and separation. Viscoelastic fluids can be synthetically formed by dissolving polymers in water or another Newtonian medium. Different polymers have been used to synthesize a viscoelastic solution for microfluidic applications including polyvinylpyrrolidone (PVP)[77], polyethylene oxide (PEO)[78–80], polyacrylamide (PAA)[81], and hyaluronic acid (HA)[82].

We previously observed that particles focus at the center of the walls due to inertial forces in a Newtonian fluid (Fig. 1-11a). This condition is achieved when the particle's Reynolds number ($Re_p = Re(a_p/L_c)^2$, where Re is the Reynolds number, a_p is the particle diameter, and L_c is the channel characteristic length or the channel's narrowest dimension) is in the order of unity. In viscoelastic fluids, an elastic force (described later in Chapter 2) is exerted on the particles in addition to the common inertial and drag forces present in non-Newtonian flows[83]. If the elastic

force is dominant on the inertial force, particles will focus at the center and the four corners of the channel (Fig. 1-11b). Finally, if the elastic and inertial forces are comparable, a 3D focusing at the center of the channel can occur (Fig. 1-11c). This phenomenon turns out to be very useful in particle separation and enhancing the separation quality of previous methods as 3D focusing is not easily achievable in Newtonian fluids.

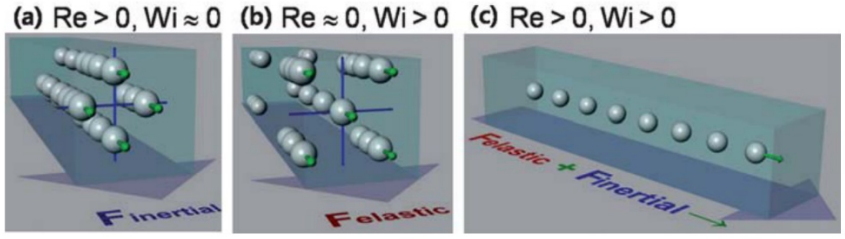

Figure 1-11 Particle focusing under (a) inertial, (b) elastic, and (c) elasto-inertial regimes[84]. These focusing situations will be described in depth in Chapter 2. Permissions obtained from RSC.

Researchers have adopted the previously developed sorting methods such as DLD[85], PFF[80], and inertial separation in straight[86] and spiral[78] channels, or introduced new techniques for separation of particles in synthetic non-Newtonian fluids like viscoelastic water. Li et al.[85] showed separation of two particles in viscoelastic fluids using the DLD method. They demonstrated that the elasticity of the fluid which affects the shear rate gives an additional means for controlling the separation process in the DLD device and thus, the critical separation size can be dynamically controlled and changed up to 40% by altering the viscoelastic properties of the fluid. Lu and Xuan[80] studied particle separation in viscoelastic flows using a microfluidic device with a pinched segment calling the method elasto-inertial pinched flow fractionation (eiPFF). They concluded that by using this method over the conventional PFF, throughput and separation resolution can be significantly enhanced due to the additional elastic force on the particles which pushes the particles to the center of the pinched section and is more effective on the larger particles and increases their separation from the smaller particles.

Faridi et al. developed a microfluidic device to separate bacteria from blood cells using inertia-elastic separation (Fig. 1-12)[30]. In this device, blood infected by bacteria and cells enters a square microchannel from two sides while a viscoelastic buffer enters the channel from the center. Blood cells which are larger than bacteria in size, focus at the center and exit the device from the center outlet, while the bacteria remain in the original stream and exit from the side outlets. This technique can be useful in the diagnosis of sepsis or Bloodstream Infections (BSI).

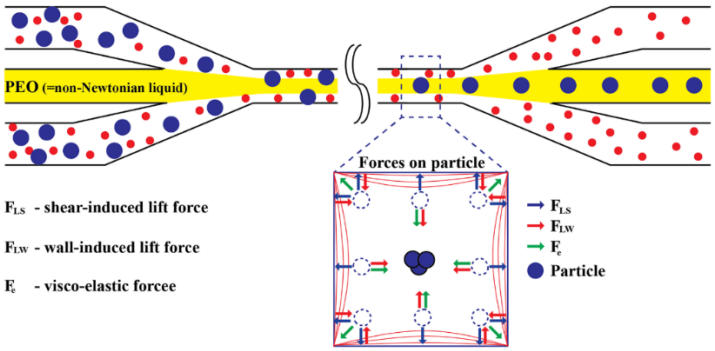

Figure 1-12 Separation of large particles (Cells) from smaller particles (bacteria) using a viscoelastic sheath flow[30].

Moreover, among the active sorting methods, magnetophoresis has been investigated in the separation of magnetic[87] and non-magnetic[88,89] particles in viscoelastic fluids. Del Giudice et al.[87] showed magnetophoresis in an H-shaped microfluidic device using a viscoelastic fluid (Fig. 1-13a). Particles entering the device from the lower inlet focus at the center of the channel due to the inertia-elastic effects. Magnetic particles deflect to the upper half of the central channel where a magnet is located and exit from the upper outlet, separating from their original solution and other non-magnetic particles. Separation of 10 µm magnetic particles from 6 µm or 20 µm non-magnetic particles were shown. Kim et al.[74] and Zhang et al.[88,89] reported sheathless particle separation using a two-step method in viscoelastic ferrofluids which elasto-inertially focuses the non-magnetic particle in a square channel, followed by magnetic deflection of magnetic particles in an expansion

zone (Fig. 1-13 b-c). However, separation of more than two particles in viscoelastic fluids has not been shown and the effect of various parameters like the magnetic field on the deflection of particles have not been deeply studied.

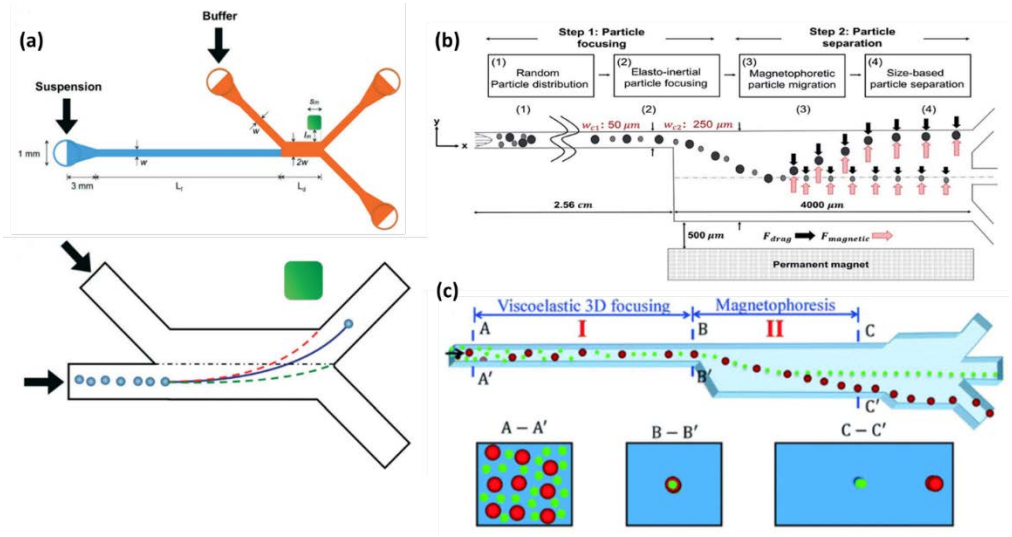

Figure 1-13 Microfluidic devices which use elasto-inertial focusing along with magnetic deflection to separate particles. (a) H-shaped which uses elasto-inertial focusing to better control the deflection of magnetic particles[87]*. (b-c) Ferrofluid based devices which use a two-step approach for separating particles. Particles first focus at the center of the long microchannel, then deflected based on their size in the expanded channel with a magnet beside it.*[88,90]*" Permissions obtained from RSC.*

1.3 RESEARCH OPPORTUNITY, GOAL AND MILESTONES

A remaining need in the field of microfluidics sample preparation is performing high-throughput, sheathless and multiplex (triplex and higher) separation of magnetic and non-magnetic particles in viscoelastic fluids with a simple design while gaining a thorough understanding of the effect of different parameters on dominant forces and particle focusing and sorting. This is required for multiplex manipulation and detection of pathogens in viscoelastic fluids in the future. Here, we have modified and applied our MIMF technique to investigate its use for parametric particle focusing studies on magnetic particles (MP) and non-magnetic particles (NMP) in viscoelastic flows. We investigated the effect of flow rate, fluid viscoelasticity, magnetic field strength, magnet

length, channel size, and expansion zone angle on the deflection of 9 and 15 µm MP and 15 µm NMP. Each of these parameters played a significant role in the final equilibrium position of particles. Our results provided the foundations for designing microfluidic devices for multiplex particle separation in viscoelastic fluids. Based on the insights gained from the parametric study, we demonstrated the triplex separation of 9 and 15 µm MPs and 15 µm NMPs. In order to prove the application of this device in separating biological targets, separation of two *E. coli* strains, immunologically attached to magnetic and non-magnetic particles, was also shown in our device. The device can potentially be used as a sample preparation tool for particle and cell separation in non-Newtonian biofluids and foods at the PoU. To achieve our goals, we pursued the following milestones.

1- Studying the physics of particle migration in viscoelastic fluids; inertial, elastic and elasto-inertial focusing; and magnetic manipulation of magnetic microparticles.
2- Identifying the shortcomings in viscoelastic particle sorting and proposing a new MIMF design based on the results of Milestones 1 and 2.
3- Devising a new method to process and quantify the results of particle focusing in our device.
4- Performing a thorough parametric study to identify the effect of the above-mentioned parameters on the focusing and deflection of magnetic and non-magnetic particles.
5- Interpreting the results using non-dimensional numbers and estimation of forces exerted on particles.
6- Identifying the best recipes to achieve triplex separation based on parametric studies and demonstrating the separation quality.

7- Implementing a protocol (Appendix A) to perform bead-bacteria conjugations and tagging two different bacterial strains to magnetic and non-magnetic particles.
8- Demonstrating the application of our device in separating bacteria using the bacteria-tagged particles from Milestone 7.

1.4 THESIS STRUCTURE

In Chapter 2, we have discussed the design of our device and the theory of elasto-inertial focusing and magnetic forces on particles as well as the non-dimensional numbers that can be used to interpret these phenomena. Also, in this chapter, we have presented the experimental setup, device fabrication, sample preparation, and data analysis processes used in Chapters 3 and 4. Chapter 3 includes the results and discussions of parametric studies on the singleplex focusing and deflection of magnetic and non-magnetic particles in our device. In Chapter 4, we have presented the Triplex-Inertia-Magneto-Elastic (TIME) sorting of particles and demonstrated the application of our device in bacterial separation. Chapter 5 presents a summary of this thesis and ideas for the future work to continue this project.

Chapter 2
THEORY AND WORKING PRINCIPLES OF THE PROPOSED MICROFLUIDIC DEVICE

2.1 MICROFLUIDIC DEVICE DESIGN AND SEPARATION THEORY

Our study focuses on investigating the effect of inertia, elastic and magnetic forces exerted on MP and NMP in viscoelastic fluids flowing at various flow rates in a magnetophoretic microfluidic device as shown in Fig. 2-1 a-c). In this device which is a modification to our MIMF device reviewed in Chapter 1, particles first reach single-point elasto-inertial focusing at the center of a square channel as shown in Fig. 2-1d. Then magnetic particles will deflect to different equilibrium positions based on their size and magneticity due to the magnetic field applied by a permanent magnet at the end of the channel, while separating into different streamlines inside an expansion region.

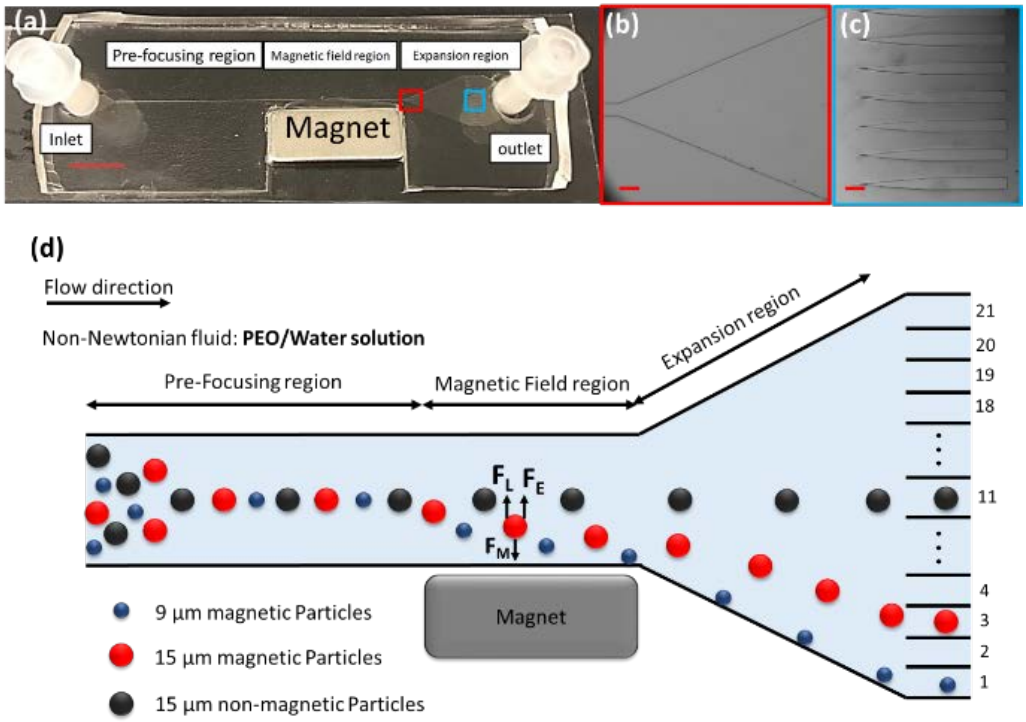

Figure 2-1 Sheathless inertia-magneto-elastic microfluidic device with Regions of Interest (ROI) shown by red and blue squares at the expansion region and the end of the channel, respectively. Scale bar=10 mm. (b) Upstream ROI under the microscope at 5x magnification which was used for singleplex particle trajectory imaging. Scale bar = 100 µm. (c) Downstream ROI under the microscope at 10x magnification showing the mini-outlet channels at the end of the expansion region (total of 21). They were used for fluorescent and optical imaging of particles during triplex sorting. Scale bar = 200 µm. (d) Schematic of the TIME sorting of 9 and 15 µm magnetic particles (MP) and 15 µm non-magnetic particles (NMP) in a viscoelastic fluid, showing the inertial (F_L), elastic (F_E) and magnetic (F_M) forces on the MP. Stokes drag force always opposes the direction of lateral motion of a particle and not shown in here.

In Newtonian fluids and under specific conditions (where particle Reynolds number is in the order of one), particles focus near the center of the walls in a square cross section channel due to the inertial force, F_L (Fig. 1-11a and Eq. 1)[91].

$$F_L = \frac{4\rho C_L {U_f}^2 a^4}{{D_h}^2}, \quad (1)$$

where C_L is a non-dimensional lift coefficient (~0.5), ρ is the solution density, U_f is the average velocity, a is the particle diameter, μ is the average solution viscosity, and D_h is the hydraulic diameter of the channel.

In viscoelastic flows at a low Re number (Eq. 2), the equilibrium position shifts to the four corners and the center of a square channel with dominance of the elastic force, F_E (Fig 1-11b and Eq. 3)[91].

$$Re = \frac{\rho U_f D_h}{\mu} = \frac{2\rho Q}{\mu(W+H)} \quad (2)$$

$$F_E = -2C_{eL}a^3\eta_p\lambda\nabla\dot{\gamma}_c{}^2 \, , \quad (3)$$

where μ is the mean viscosity of the fluid, Q is the flow rate, and H and W are the channel height and width, respectively. In Eq. 3, C_{eL} is a non-dimensional elastic lift coefficient, η_p is the part of the solution viscosity that can be related to the polymeric contribution, λ is the fluid relaxation time, and $\dot{\gamma}_c$ is the shear rate. If the Re number is high enough in a viscoelastic flow so that inertial force acts on the particles in the same order as the elastic force, the balance of these two forces will reduce the equilibrium positions into one at the center of the square channel as shown in Fig. 1-11c.

The elastic lift force develops due to the changes in the normal stress differences in viscoelastic flows[92]. First normal stress difference can be shown as $N_1 = \tau_{11} - \tau_{22}$ which acts along the streamlines and second normal stress difference can be shown as $N_2 = \tau_{22} - \tau_{33}$ which acts on the channel cross-section direction. Since the magnitude of the second normal stress difference is much smaller than the first normal stress difference, we can approximate the elastic lift force by only considering the N_1. When particles focus solely due to the presence of F_E, the equilibrium positions are where the gradient of N_1 is minimum. These positions in a square channel are at the center of the channel and the four corners (Fig. 2-2a)[93]. Simultaneous acting of inertial and elastic forces on particles can lead to single-line 3D focusing at the center-point in a straight square channel as the higher flow rate can eliminate the local minima of the shear gradient at the corners of the channel (Fig. 1-11c and 2-2)[84].

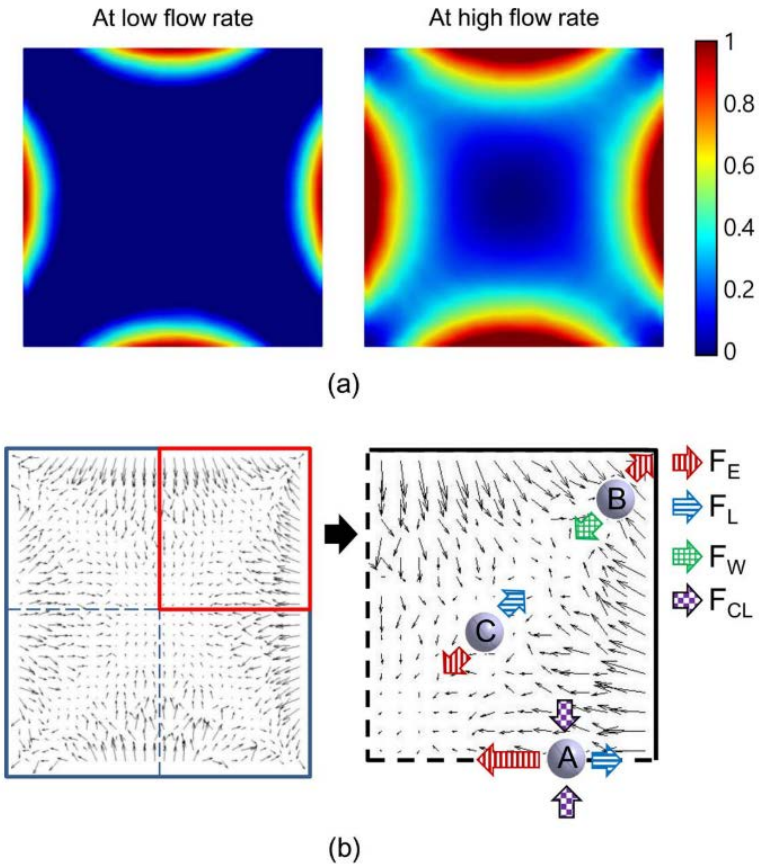

Figure 2-2 (a) Distribution of the square of shear rate at low and high flow rates. At high flow rate, there are 5 points at 4 corners and the center of the channel where the square of shear rate and its gradient are minimum. (b) Vectors showing the direction and magnitude of elastic forces. F_E, F_L, F_W, and F_{CL} show the elastic lift force, inertial lift force, wall repulsion and inertial cross-lateral forces, respectively[93]. Permissions obtained from AIP.

If a magnet is positioned beside the channel and magnetic particles are used as in Fig. 2-1, then a magnetic force, F_M, towards the magnet (Eq. 4) will be applied to the flowing particles[58].

$$\vec{F}_M = \frac{4\pi}{3} M r^3 \nabla B, \tag{4}$$

where M is the magnetization, r is the particle radius ($r = a/2$), and B is the magnetic field. Magnetization can be calculated as $M = \frac{\nabla \chi \, B}{\mu_0}$. It is linearly dependent on the magnetic field strength as the difference in magnetic susceptibility of MPs and the medium, $\nabla\chi$, and the permeability of vacuum, μ_0, are both constant. It should be noted that for particles moving with velocity V_p in the

lateral direction of the channel, an additional stokes drag force ($F_S = 3\pi\mu a V_p$) will also be applied opposing the particle's direction of motion. Particles at equilibrium will no longer experience this drag force because V_p=0 at the equilibrium.

For viscoelasticity of a fluid in a microchannel, a non-dimensional number called the Weissenberg number (Wi) in Eq. 5 can be used[94]. Re number indicates the ratio between inertial and viscous forces while Wi demonstrates the ratio of elastic and viscous forces.

$$Wi = \lambda \dot{\gamma}_c \,, \tag{5}$$

At mean viscosity, the average shear rate in a rectangular channel can be expressed as $\dot{\gamma}_c = 2Q/HW^2$. Therefore, Wi number can be simplified as shown in Eq. 6.

$$Wi = \frac{2\lambda Q}{HW^2} \tag{6}$$

Inertia-elastic focusing can be characterized by finding the ratio of Wi number to the Re number which shows the relationship between the strength of elastic forces and inertial forces. This ratio is called the Elasticity number (El) and can be calculated for a rectangular channel as shown in Eq. 7.

$$El = \frac{Wi}{Re} = \frac{\lambda\mu(W+H)}{\rho W^2 H} \tag{7}$$

Wi and Re are linearly dependent on the flow rate. Therefore, their ratio, El, will be independent from the flow rate and only depends on the fluid properties and channel dimensions. By knowing the magnitude of the inertial force (Eq. 1) and the El number (Eq. 7) in a channel, the elastic force can be estimated indirectly even if C_{el} and η_p are unknown. In order to reach single-line inertia-elastic focusing in a square channel, El needs to be approximately in the order of unity (O(1)).[84]

Single-line focusing is less likely to be achieved as the El number increases or decreases (Fig. 1-11).

2.2 WORKING PRINCIPLES OF THE MICROFLUIDIC DEVICE

Based on the above theory, the working condition of our device is where the inertial and elastic forces first focus the MP and NMP in the pre-focusing region. Based on our calculations[95] and as shown in Appendix B, in the worst case scenario, this can be achieved within 21.97 mm for our smallest 9 μm MP at the lowest flow rate of 0.25 mL/hr and PEO concentration of 500 ppm, in the largest microchannel (90 μm×90 μm cross section). This length is shorter than the length of the pre-focusing region (32 mm) in Fig. 2-1d. The magnetic particles gain different equilibrium positions based on their sizes at the magnetic field region due to the application of the magnetic force towards the sidewall of the channel. The position of particles can then be observed and imaged at the expansion zone or in the mini-outlets of the device. Based on the equations provided in the previous section, we have used the non-dimensional numbers and a force analysis approach to discuss the results obtained for the MPs and NMPs in our device. As a rough estimate, all forces were assumed to be in the horizontal plane.

2.3 EXPERIMENTAL METHODS

2.3.1 Sample Preparation

The non-Newtonian fluid was prepared by mixing Poly(ethylene oxide) (PEO) powder (average Mv of 200,000 Da, Sigma Aldrich, USA) in DI-water at different concentrations of 500, 1000, and 2000 ppm. The zero shear viscosities for these concentrations are 1.8, 2.3 and 4.1 mPa.s,

respectively (as reported by Lu et al. [96]). The PEO powder was dissolved in water by stirring overnight at room temperature. Our experiments were performed using MP with the diameter of 9 µm (CM-80-10, 8-9.9 µm) and 15 µm (CM-150-10, 14-17.9 µm) from Spherotech Inc., USA and NMPs with the diameter of 15 µm (1015KB, blue color dyed polystyrene) from Phosphorex Inc., USA. For triplex sorting, 15 µm green fluorescent non-magnetic particles (Phosphorex 2106G), 9 µm red fluorescent magnetic particles (Spherotech FCM-8056-2, 8-9.9 µm), and the above-mentioned 15 µm non-fluorescent MP were used. The ratio of particle solution and PEO-water solution were chosen in a way to obtain ~10^6 particles per mL in each experiment. A small amount (0.5% v/v) of Tween 20 (Sigma Aldrich, USA) was added to the solutions to prevent particles from aggregation.

To prepare the bead-bacteria solution (see Appendix A for standard operation procedures), liquid cultures of *E. coli* K12 JM83 (resistant to Streptomycin) and *E. coli* BL21 were prepared in LB solution (L3522, Sigma-Aldrich, MO, US) and incubated in 37° overnight. Meanwhile, separate 100 µl solutions of Streptavidin-coated 9 µm MP (SVM-80-5, 8.0-9.9 µm) and 15 µm NMP (SVP-150-4, 14.0-17.9 µm) from Spherotech Inc., USA were prepared and washed three times with 1 mL PBS (P4417, Sigma Aldrich) +0.1% BSA (A8412, Sigma-Aldrich). 5 µl of anti-*E. coli* biotinylated antibody (ab20640, Abcam, Cambridge, UK) was added to each particle solution and incubated for 60 minutes with gentle rotation. Particles were washed 5 times with PBS+0.1% BSA to remove unbound antibodies. At the end of the wash step, 1 mL of bacteria culture was added to the particle solution and incubated for 60 minutes with gentle rotation. The JM83 bacteria were mixed with 9 µm MP and the BL21 bacteria were mixed with 15 µm NMP. Serially-diluted samples of the prepared bacteria stocks were cultured on MacConkey agar (B11387, Fisher Scientific, NH, US) plates. After incubation, MPs were immobilized by placing beside a magnet,

NMPs were immobilized by centrifugation, and the supernatant was taken out and cultured to count the unattached bacteria. The bead-bacteria solutions were washed 5 times with PBS+0.1% BSA and the last washed sample was resuspended in PBS+PEO solution for testing. Diluted portions of these solutions were cultured on MAC agar plates to characterize the attached bacteria.

2.3.2 Device Design and Fabrication

The microfluidic device shown in Fig. 2-1 a-c consisted of an inlet, a straight square channel with various dimensions, a symmetric expansion zone with various expansion angles, and 20 flow separators at the end of the expansion zone forming 21 mini-outlets. For simplicity of singleplex experiments in Chapter 3, the mini-outlets were rejoined into one outlet at the end of the device. For particle and bacteria separation in Chapter 4, a triple outlet device was used in which the first outlet consisted of the mini-outlets 1-9, second outlet consisted of the mini-outlets 10-12, and the third outlet consisted of mini-outlets 13-21.

A rare-earth Neodymium-Iron-Boron (NdFeB) magnet (Indigo Instruments, ON, Canada) was placed beside the narrow channel right before the expansion region. Six magnet configurations were chosen to investigate the effect of magnetic field strength and exposure length. The investigated magnetic field strengths were approximately 100, 200, and 300 mT measured by a Gaussmeter (GM07, Hirst Magnetics, Cornwall, UK). Magnet sizes, and hence the exposure lengths, were 12.5 and 25 mm. In order to investigate the effect of channel dimensions, square cross-section narrow channels with 70 and 90 μm width/height and a 45° transition angle to a 10 mm wide expansion zone were designed. To examine the effect of the transition angle on particle deflection and dispersion, we fabricated the 90 μm channel device with two more expansion zone angles of 30° and 60°.

The device layouts were designed in the AutoCAD software and printed on photomasks by CAD/Art Services, Inc., OR, USA. The device master molds were fabricated using photolithography. SU-8 2075 photoresist (Microchem Corp., MA, USA) was spun on silicon wafers with the diameter of 4 inches (Wafer World Inc., FL, USA) using a spin coater (200DBX Develop-Bake System, Brewer Science, Cost Effective Equipment, MO, USA). Then, the molds were pre-baked on hot plates at 65°C and 95°C based on Microchem's data sheet. SU8 coated wafers were exposed to UV light (UV KUB 2, Kloé, Montpellier, FR) through the photomasks. After post baking the UV-exposed molds at 65°C and 95°C, they were washed with SU-8 developer to dissolve the unexposed SU-8 on the silicon wafers. The molds were finally hard-baked at 150°C for 30 minutes.

The molds were then used to fabricate the microfluidic devices using soft-lithography[97]. Polydimethylsiloxane (PDMS, Dow Corning Sylgard 184 Silicone, Ellsworth Adhesives, ON, Canada) was mixed at 1:10 ratio of base to curing agent and poured over the SU-8 molds with inlet and outlet tubes installed in place on top of channel reservoirs. A 25 mm-long magnet replica was also placed beside the end of the narrow channel to replicate the space for placing the magnet. The PDMS prepolymer was cured at 80°C for 4 hr, then peeled off the mold and bonded to a glass slide (Brain Research Laboratories, MA, USA) using an oxygen plasma machine (Harrick Plasma, PDC-001, NY, USA). The permanent magnet was placed in the replicated empty space before bonding the PDMS to glass.

2.3.3 Experimental Setup and Procedure

The experimental setup consisted of one of the microfluidic devices tested under an inverted fluorescent microscope (BIM500FL, Bioimager, ON, Canada). Singleplex samples of suspended

microparticles inside PEO-water solutions were prepared as previously described and flown into the device at various flow rates of 0.25-1.5 mL/hr using a syringe pump (KD Scientific Inc., MA, USA). For TIME sorting, 9 μm RFP MP, 15 μm non-fluorescent MP, and 15 μm GFP NMP were mixed in 1000 and 2000 ppm PEO-water solutions and tested at 1.5 mL/hr in the 90 μm cross section device. Stacks of optical and fluorescent images were taken from the expansion region or the mini-outlets of the device using the inverted microscope with a camera (Point Grey, FLIR Integrated Imaging Solutions Inc., BC, Canada) at 22 fps.

For bacterial separation, the prepared bead-bacteria solutions were mixed together and 10x and 100x dilutions were prepared. These solutions were run through the triple outlet device at optimal recipes obtained from our singleplex and triplex particles studies. Outlet reservoirs were used to maintain the same back pressure in all the outlets. The output solutions collected from each reservoir were serially diluted and cultured on two MAC agar plate, with and without Streptomycin (S9137, Sigma-Aldrich). The number of colonies on each plate were counted after 24 hours and used for back-calculating the bacterial concentrations needed to characterize the sorting purity and efficiency of our device.

2.3.4 Data Analysis

In singleplex experiments, up to 500 frames obtained per experimental condition were overlapped using the MATLAB Image Processing tool, as shown in Fig. 2-3 for 9 μm MP in water and 2000 ppm PEO-water, inside the 90μm device with and without a magnet. The MATLAB code selected the first frame as the background image and subtracted it from the rest of the images, then stacked them all to produce a single image. The difference of each frame from the first frame would be the particles that moved in the channel and the particles that entered the camera's field of view. To

find the equilibrium position of the particles in the expansion zone, the color intensity of a vertical line at a distance of ~400 µm from the start of the expansion zone was measured by the open-source ImageJ software[98]. To find the center point of the deflected particle stream and the dispersion of particles, normalized intensity data (by the width of the scanning line, H) were analyzed, by fitting a Gaussian curve onto the intensity points (Fig. 2-3d). The center of the fitted curve showed the position of the particles in the channel and the diagram's full width at half maximum (FWHM) was used as a measure of particle dispersion[51] and shown as error bars in the graphs.

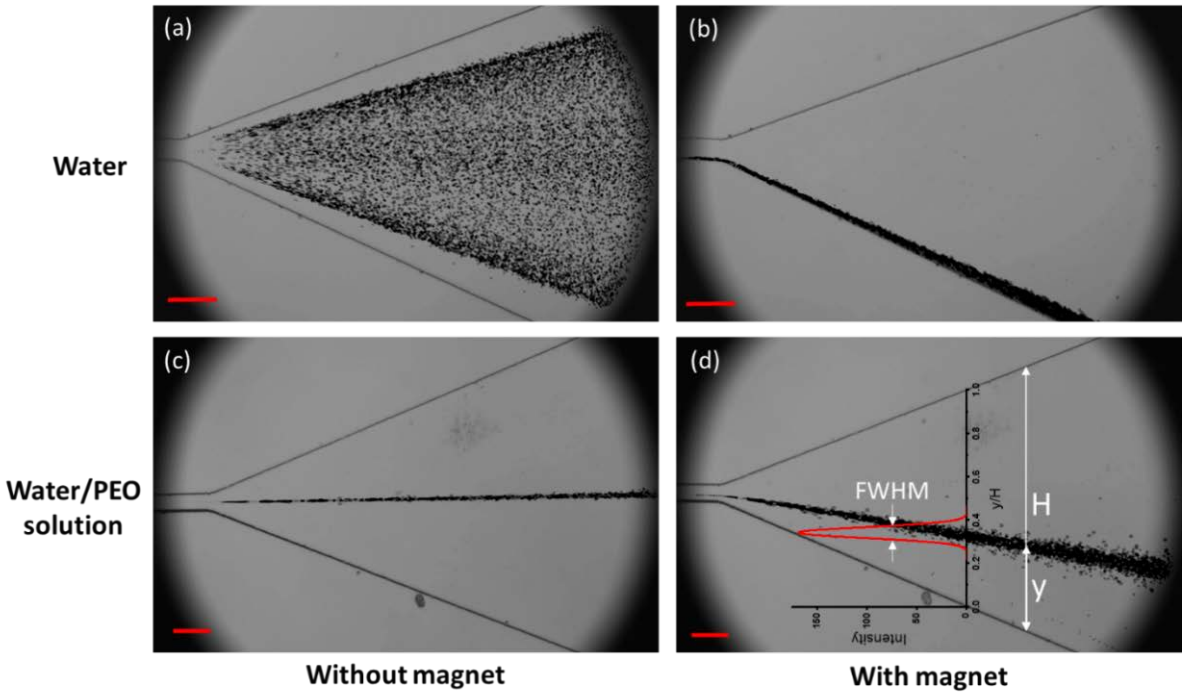

Figure 2-3 Overlapped images (up to 500 frames) of inertia-magneto-elastic focusing of 9 µm magnetic particles at 1 mL/hr flow rate of (a) water without a magnet, (b) water with a 12.5 mm long magnet and magnetic field of 200 mT, (c) 2000 ppm PEO solution without a magnet, and (d) 2000 ppm PEO solution with a 12.5 mm long magnet and magnetic field of 200 mT. The fitted Gaussian intensity curve measured at a line 400 µm away from the expansion zone entrance is shown in (d) with full width at half maximum (FWHM) used as a measure for particle dispersion (scale bars = 200 µm).

In TIME sorting experiments, we counted the number of particles passing through the mini-outlet channels shown in Fig. 2-1c during a maximum 10 s time interval. The time intervals were shorter in cases where particles had high concentration and 500 particles were counted passing the outlets

each time. For this, the Analyze Particles module in ImageJ was used to count the number of particles with the same pixel size in the brightfield, GFP and RFP images acquired separately at each mini-outlet. The effect of recording at various times was minimized by repeating each experiment three times and ensuring that the sample contained a homogeneous and time-independent distribution of particles. The numbers of particles counted in each mini-outlet were normalized by the total number of each particle in all outlets. The efficiency and purity of sorting for each particle were calculated in the outlets where they were dominated by using Eq. 8 and Eq. 9[99].

$$\text{Purity} = \frac{\text{\# of Target Particles Sorted in Selected Mini-Outlets}}{\text{Total \# of All Particles in Selected Mini-Outlets}} \times 100 \quad (8)$$

$$\text{Efficiency} = \frac{\text{\# of Target Particles Sorted in Selected Mini-Outlets}}{\text{Total \# of Target Particles in All Mini-Outlets}} \times 100 \quad (9)$$

Data analysis for bacteria separation was done by calculating the concentrations of bacteria at each step before and after separation in the device. These concentrations were calculated by counting the number of colony-forming units (CFU) on the plates described in Section 2.3.1 and using Eq. 10.

$$Bacteria\ Concentration\left(\frac{CFU}{ml}\right) = \frac{CFU\ counted}{dilution\ factor \times Sample\ Volume\ (ml)} \quad (10)$$

The calculated concentrations were then used to calculate the purity and efficiency using Eq. (8) and (9). Recovery rate was defined as the ratio of the bead-bacteria concentration collected from the device at a desired outlet to the concentration of the same bead-bacteria in the input solution.

Chapter 3

PARAMETRIC STUDY OF MICROPARTICLE FOCUSING IN NON-NEWTONIAN FLUIDS

3.1 SINGLEPLEX BEHAVIOR OF MICROPARTICLES IN THE DEVICE

We started our investigations by examining the behaviour of 9 µm MP in water with and without a magnet in the 90 µm channel as a proof of concept experiment. As shown in Fig. 2-3a, the particles were relatively dispersed in the channel when flown at 1 mL/hr with a slight enhanced concentration at the edges of the dispersion band. Applying a 200 mT magnetic field with a 12.5 mm long permanent magnet resulted in particles attraction all the way towards the sidewall of the channel (Fig. 2-3b). In Fig. 2-3c, the effect of adding the viscoelasticity effect to the solution is shown by examining the dispersion of 9 µm MP in 2000 ppm PEO-water solution at 1 mL/hr with no magnet. This resulted in the elasto-inertial focusing of particles at the center of the channel. A

magnet beside the channel in this case attracted the particles to a new equilibrium position other than the center point and away from the sidewall (Fig. 2-3d).

To characterize the deflection of particles for future particle sorting, we investigated the effect of flow rate (affecting inertial and elastic forces), PEO concentration (affecting relaxation time and the elastic force), magnetic field strength and exposure length (affecting magnetic force), channel size (affecting inertial and elastic forces), and expansion zone angle (presumably affecting particle dispersion) on the focusing and deflection of 9 and 15 µm MP and 15 µm NMP. For these parametric studies, flow rate, PEO concentration, magnetic field strength, magnet length, channel size, and expansion zone angle were selected at base values reported in Table 1.

Table 1. Base configurations used in parametric studies

Parameter	Flow Rate	PEO Concentration	Magnetic Field Strength	Magnet Exposure Length	Channel Width and Height	Expansion Zone Angle
Magnitude	1.5 mL/hr	2000 ppm	200 mT	12.5 mm	90 µm	45º

3.1.1 Effect of Magnetic Field Exposure Length

We first studied the effect of magnetic force exposure length (at 200 mT) on the position of 9 and 15 µm MPs and 15 µm NMPs. As expected, all three particles focused at the center of the channel (y/H = 0.5) when no magnet was used in the device as shown in Fig. 3-1.

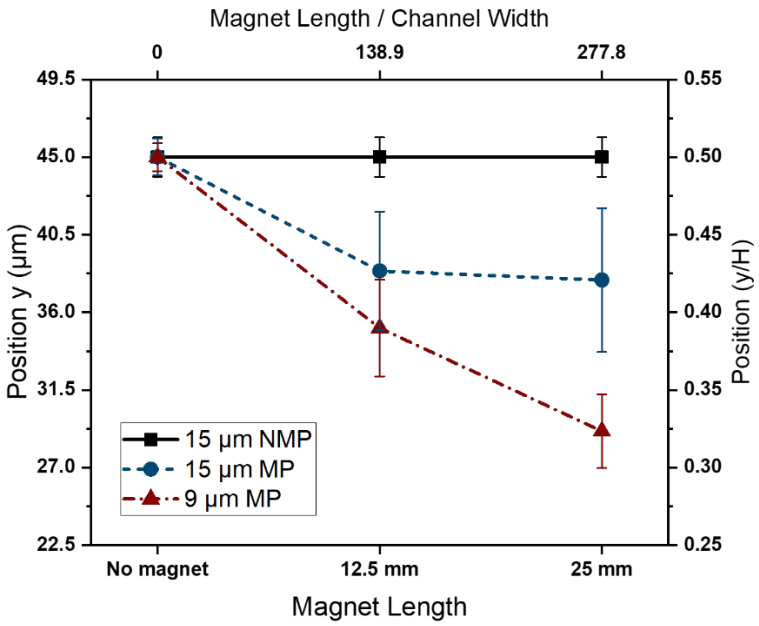

Figure 3-1 The effect of magnetic force exposure length on particle deflection where flow rate was 1.5 mL/hr, magnetic field strength was 200 mT, PEO concentration was 2000 ppm and channel width and height were 90 µm.

Keeping the flow rate and PEO concentration constant, adding a 12.5 mm long magnet beside the channel resulted in deflection of the MP toward the sidewall (Fig. 3-1), while the 15 µm MPs were closer to the center (initial focusing point) than the 9 µm MPs. The magnetic field did not have any impact on the NMPs, as anticipated. When the 12.5 mm long magnet was replaced by a 25 mm long magnet, MPs were pulled further towards the sidewall. By comparing the position of 9 and 15 µm MPs with 12.5- and 25-mm long magnets, it can be seen that the effect of a longer magnet is more significant on the 9 µm MP. Also, the dispersion of the 15 µm MP slightly increased while the 9 µm MPs remained more focused. Fig. 3-1 also shows that the 25 mm magnet with a magnetic field of 200 mT at a flow rate of 1.5 mL/hr is one of the potential conditions in which separation of the three particles can be obtained.

3.1.2 Effect of Magnetic Field Strength

The next objective was to study the effect of magnetic field strength on the position of MPs and examine if any of the particles reach magnetic saturation, meaning that they stop deflecting further towards the sidewall as the magnetic field strength increases. The magnet length was set at 12.5 mm and magnetic field strength was changed from 100 to 300 mT (Fig. 3-2). Other parameters were set according to Table 1.

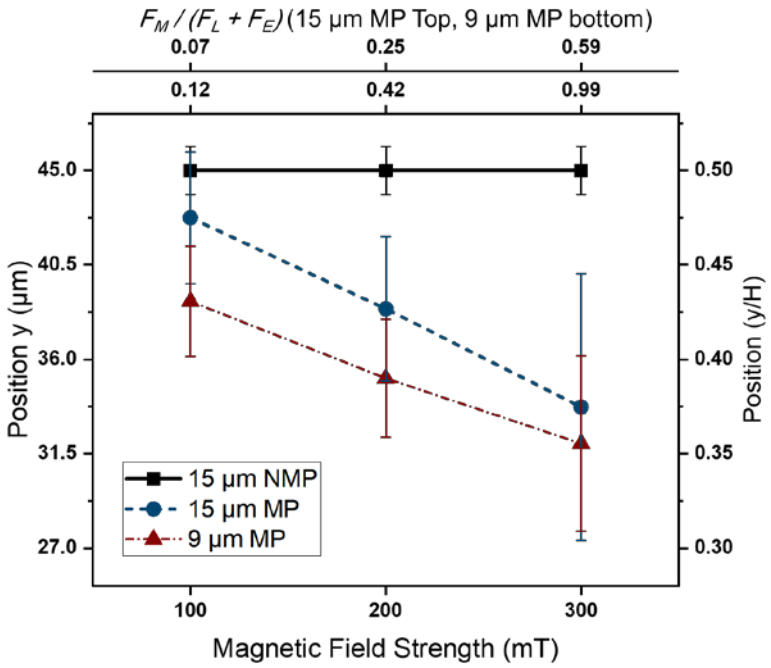

Figure 3-2 The effect of magnetic field strength on particle deflection where flowrate was 1.5 mL/hr, magnetic field exposure length was 12.5 mm, PEO concentration was 2000 ppm and channel width and height were 90 µm.

It can be seen from Fig. 3-2 that while increasing the magnetic field strength had an almost linear effect on the deflection of MPs, its effect on 9 µm MPs was slightly lower than 15 µm MPs. This resulted in a smaller distance between the two particle streams at 300 mT. Also, increasing the magnetic field strength resulted in higher dispersion of MPs, particularly the 15 µm MPs. Considering the overlap with the NMPs, one can conclude that the average magnetic field of 200 mT may be preferable for a triplex sorting device.

3.1.3 Effect of Flow Rate

The next studied parameter was the flow rate, which was changed from 0.25 mL/hr to 1.5 mL/hr with 0.25 mL/hr intervals, keeping the other parameters at the base values in Table 1. In addition to the effect of flow rate on the MPs deflection, another question was whether the NMPs stay focused as the flow rate decreases and the effects of inertial and elastic focusing diminish based on Eqs 1 and 3. Results are demonstrated in Fig. 3-3 for the three tested particles.

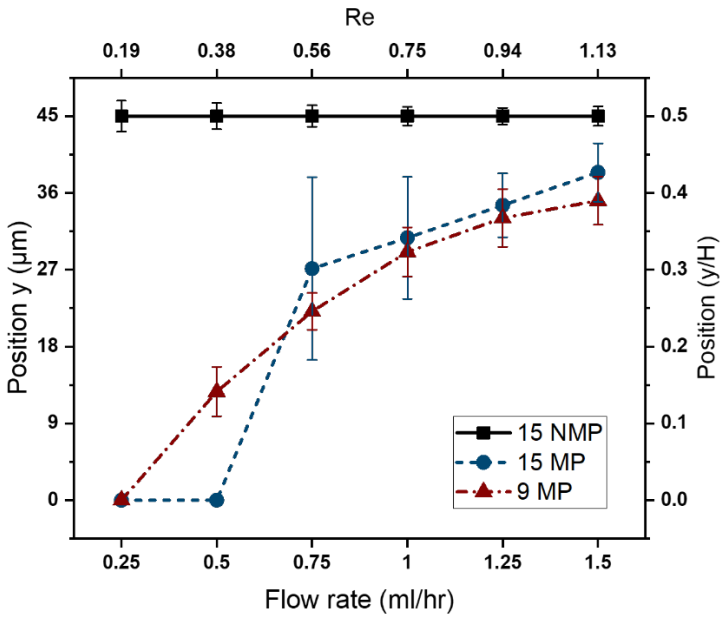

Figure 3-3 The effect of flow rate on particle deflection where magnetic field strength was 200 mT, magnetic field exposure length was 12.5 mm, PEO concentration was 2000 ppm and channel width and height were 90 µm.

Fig. 3-3 shows that both 9 and 15 µm MPs deflected more toward the wall as the flow rate was decreased, reaching to a complete deflection to the channel sidewall (y/H = 0) at the flow rate of 0.25 mL/hr. However, the trends were not similar for both particles. The larger 15 µm MP showed a linear shift in position towards the wall as the flow rate was decreased from 1.5 mL/hr to 0.75 mL/hr, followed by a sudden attraction to the channel sidewall at lower flow rates of 0.25-0.5 mL/hr. However, the 9 µm MPs showed a gradual and steady decrease of distance from the sidewall with reduction in the flow rate. Also, by decreasing the flow rate, the dispersion of 15 µm

MPs was drastically increased in the linear region, while it was almost constant for 9 µm MPs. Particle dispersion diminished significantly for all cases where magnetic focusing at the sidewall was obtained. As for the 15 µm NMPs, they kept focusing at the center of the channel, although the focusing quality was slightly decreased at flow rates higher than 1.25 mL/hr or lower than 1 mL/hr.

3.1.4 Effect of Viscoelasticity

The effect of viscoelasticity was examined by changing the fluid's relaxation time (Eq. 5). This was done by testing PEO-water solutions at three different concentrations of 500, 1000, and 2000 ppm PEO (Fig. 3-3). Other parameters were kept at the base configurations of Table 1.

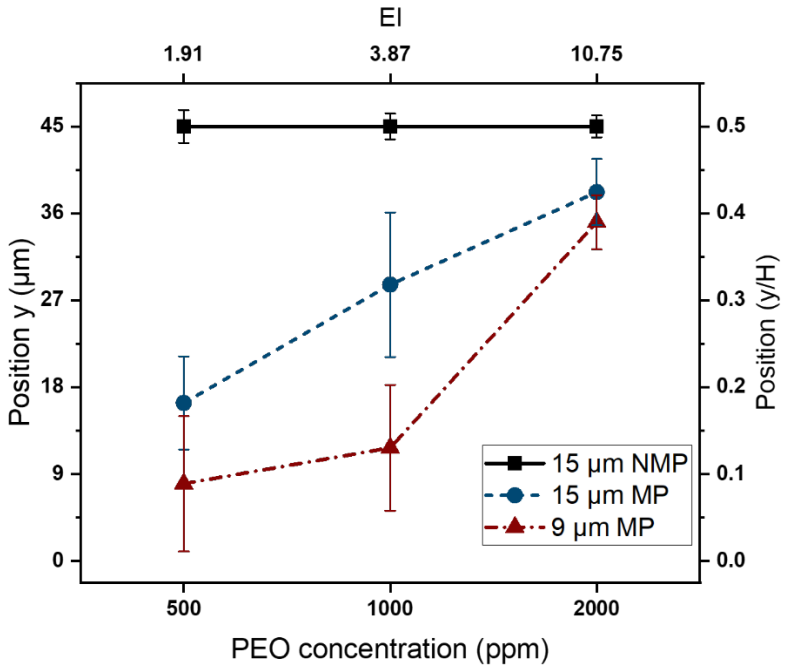

Figure 3-4 The effect of PEO concentration on particle deflection where flowrate was 1.5 mL/hr, magnetic field strength was 200 mT, magnetic field exposure length was 12.5 mm, and channel width and height were 90 µm.

Fig. 3-4 shows the MPs deflecting more toward the channel sidewall as the PEO concentration was decreased. NMPs stay focused at the channel centerline at all three concentrations. Also, the

dispersion of all particles slightly increased as the PEO concentration was decreased. The possibility of triplex separation can be observed in a 1000 ppm PEO-water solution at a flow rate of 1.5 mL/hr using a 12.5 mm-long 200 mT magnet in our setup.

3.1.5 Effect of Channel Dimensions

A parameter that affects the *Re* and *El* numbers is the channel dimensions. Therefore, our studies above were repeated for a smaller square microchannel with 70 µm width and height, using a 12.5 mm long magnet with 200 mT of magnetic strength. The results are presented in Fig. 3-5 based on the flow rate for each particle.

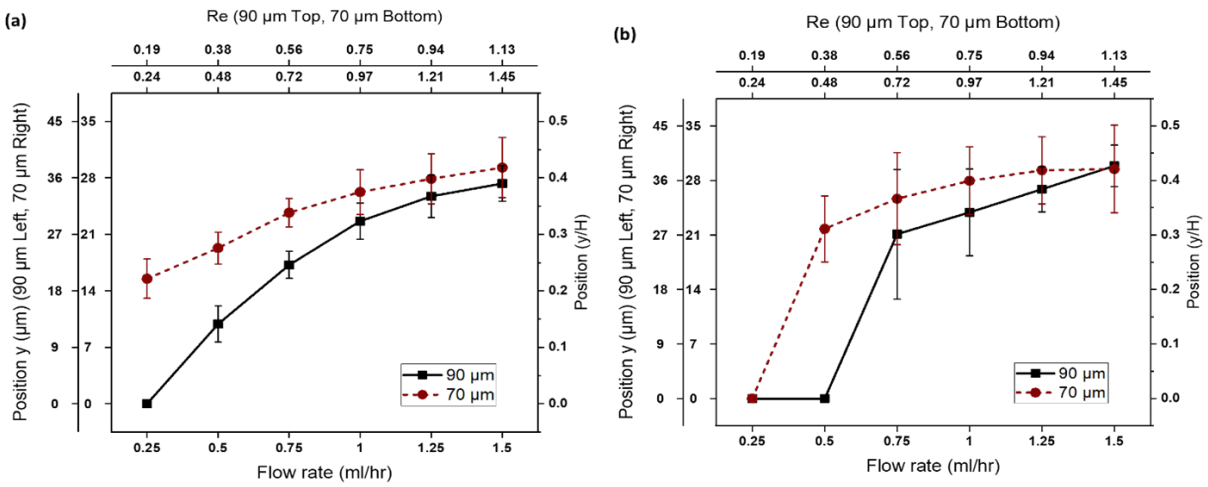

Figure 3-5 The effect of square channel width and height of 70 µm or 90 µm (legends) on the deflection of (a) 9 µm MPs and (b) 15 µm MPs, where PEO concentration was 2000 ppm, magnetic field strength was 200 mT, and magnetic field exposure length was 12.5 mm. NMPs were always focused at the channel center line with y/H=0.5 (data not shown).

It can be seen in Fig. 3-5 that both MPs tend to stay closer to the center in the smaller 70 µm microchannel, while showing the same trend of shifting towards the sidewall as the flow rate was decreased from 1.5 mL/hr to 0.25 mL/hr. The NMPs focused at the center of the channel in both channels and at all the flow rate (data not shown), while they showed slightly less dispersion in the 70 µm microchannel.

3.1.6 Effect of Expansion Zone Angle

Finally, to examine whether the expansion zone angle had an effect on the position and dispersion of particles, experiments were repeated with 90 µm microchannel devices with 30- and 60-degrees expansion angles, in a 2000 ppm PEO-water solution with a 12.5 mm long magnet at 200 mT of magnetic field (Fig. 3-6).

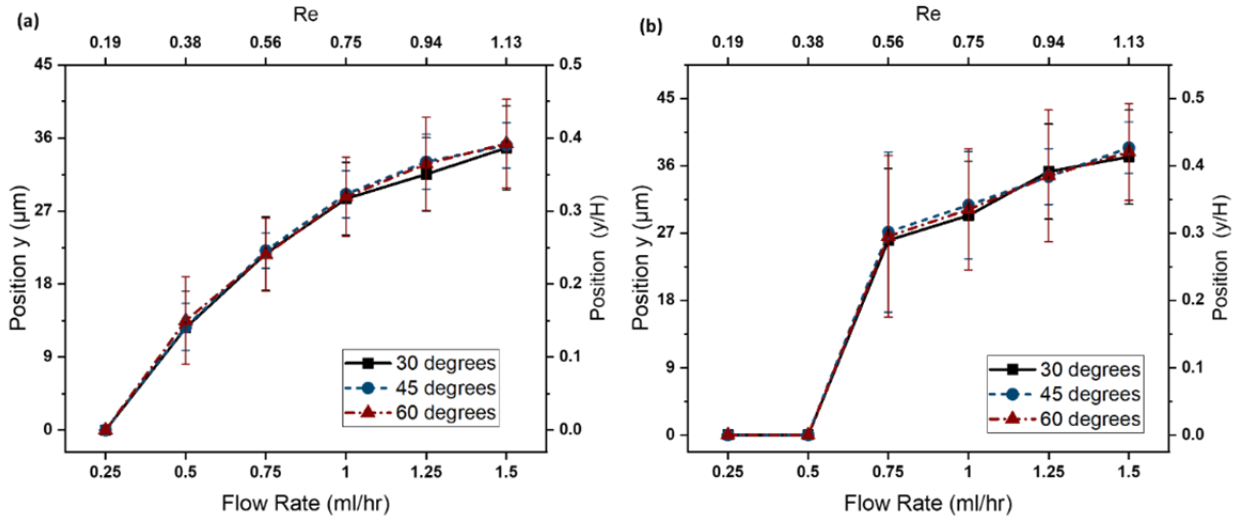

Figure 3-6 The effect of expansion angle on the deflection of (a) 9 µm MP and (b) 15 µm MP, where PEO concentration was 2000 ppm, magnetic field strength was 200 mT, and magnetic field exposure length was 12.5 mm. Microchannel width and height were 90 µm. NMPs were always focused at the channel center line with y/H=0.5 (data not shown).

The results in Fig. 3-6 do not show a significant difference in the normalized position of MPs and NMPs due to the change in the expansion angle of the device. The particle dispersion slightly differs between the three devices with the 45 degrees angle device showing the least and 60 degrees angle device showing the highest dispersion.

3.2 DISCUSSION

In this section, we will use the theory provided in Chapter 2 to calculate the non-dimensional numbers and estimate the magnitude of the elastic, inertial and magnetic forces in order to discuss the outcomes of the experiments presented in Section 3.1.

Particles in a square channel inertially focus near the center of the walls when the carrier fluid is Newtonian. However, with a certain channel size and particle diameter, a relatively high flow rate is needed to make the inertial force significant enough to completely focus the particles. It is known that the particle Reynolds number ($Re_p=Re(a/D_h)^2$) should be greater than unity to achieve inertial focusing in a channel[71,72]. In our 90 µm square microchannel, the particle Reynolds number for 9 µm MPs at a flow rate of 1.5 mL/hr in water was ~0.05. As a result, particles were dispersed in the channel with a slightly higher concentration at the wall centers, mainly because inertial forces were not strong enough ($F_L=\sim1.9\times10^{-12}$ N) to focus the particles at their equilibrium positions (Fig. 2-3a). In this case, adding a 200 mT magnetic field at the side of the channel resulted in deflecting all the MPs towards the channel sidewall, since the magnetic force ($F_M=\sim2.1\times10^{-11}$ N) was dominant by an order of magnitude over the inertial force.

Adding viscoelasticity to the water can help the particles reach single-point elasto-inertial focusing when elastic and inertial forces are comparable, and the El number is not much higher or lower than unity. In our 90 µm microchannel, the El number was 10.75 when the PEO concentration was 2000 ppm ($F_E=\sim2\times10^{-11}$ N for 9 µm MPs in Fig. 2-3c). In this case, the particles focused perfectly at the center of the channel (Fig. 2-3c). The magnetic force exerted from a 200 mT magnetic field to the 9 µm MPs ($F_M=\sim2.1\times10^{-11}$ N) was comparable to the elastic force which transferred the 9 µm MPs from the center of the channel to a new equilibrium position as shown in Fig. 2-3d. In

fact, multiple parameters can be changed to modify the magnitude of these forces and consequently alter the resultant equilibrium position of each particle.

In Fig. 3-1 and for the experiment without a magnet, all MPs and NMPs focused at the center of the channel due to the El number of 10.75 and the dominance of the elastic forces. With the magnet, 9 and 15 µm MP moved closer to the wall with 9 µm MP deflecting more than 15 µm MP. The forces exerted on these particles are highly dependent on particle diameter, a. Magnetic and elastic forces scale with a^3, while the inertial force is dependent on a^4. As a result, the sum of forces keeping the particles at the center are higher for 15 µm MP than 9 µm MP (e.g. $\sum F_{15MP} = 3.1 \times 10^{-10}\ N$ vs $\sum F_{9MP} = 3.4 \times 10^{-11}\ N$ for the 25 mm long magnet). This results in 15 µm MPs focusing at a closer distance to the NMPs. The length of the magnet also determines the time that the particles are exposed to the magnetic field and using a longer magnet means that the particles have more time to move towards the sidewall, hence a larger deflection seen for the 25 mm long magnet in Fig. 3-1. The higher dispersion of 15 µm MP can be attributed to their wider size distribution, i.e. 14 – 17.9 µm for 15 µm MP compared to 8 – 9.9 µm for 9 µm MP as reported by their manufacturer. This difference in size can make the magnitude of the forces variable among the particles resulting in their dispersion within a focused particle stream. This parameter could not be controlled due to the limitations in commercially available particles, but based on our results, we expect monodispersity of size to be a highly effective factor in acquiring a focused beam of particles.

The effect of magnetic field strength is shown in Fig. 3-2. By using a higher magnetic field strength and according to Eq. 4, magnetic force would grow larger due to an increase in magnetization, M, and magnetic field gradient, ∇B. Magnetization for 100, 200, and 300 mT magnetic fields were calculated to be 9×10^5, 1.8×10^6, and 2.7×10^6 A/m, respectively. ∇B for 100, 200, and 300

mT magnetic fields in the horizontal plane were measured with a gaussmeter with magnitudes of 8, 23.7, and 31.6 T/m for the 25 mm long magnet, and 16.6, 30.5, and 48.1 T/m for the 12.5 mm long magnet, respectively. To provide an example, the sum of inertial and elastic forces on 15 µm MP in all conditions of Fig. 3-2 was $\sum(F_L + F_E)_{15MP} = 3.88 \times 10^{-10}\ N$, while the magnetic force increased from $F_M = 2.8 \times 10^{-11} N$ to $F_M = 2.3 \times 10^{-10}\ N$ as the magnetic field was increased from 100 mT to 300 mT. Hence, the magnetic force magnitude became comparable to the sum of elastic and inertial forces and the particles moved closer to the wall. It is known that the particles will reach magnetic saturation when the magnetic field increases beyond a threshold[58]. Therefore, to avoid reaching saturation, having less dispersion and more distinction between the particles, using lower magnetic field strengths will be suitable. We did not observe magnetic saturation in our experiments as the MPs continued deflecting towards the sidewall with increase in the magnetic field strength.

According to Eq. 1 and Eq. 3, flow rate affects the magnitude of both inertial and elastic forces. By decreasing the flow rate, inertial and elastic forces decrease, and the magnetic force becomes comparable on MPs, while the MPs also get a longer exposure to the magnet and deflect further towards the channel sidewall as seen in Fig. 3-3. For instance, at Q=1.5 mL/hr, $\sum(F_L + F_E)_{15MP} = 3.88 \times 10^{-10}\ N$ and $\sum(F_L + F_E)_{9MP} = 5.03 \times 10^{-11}\ N$, while at Q=0.25 mL/hr, $\sum(F_L + F_E)_{15MP} = 1.08 \times 10^{-11}\ N$ and $\sum(F_L + F_E)_{9MP} = 1.4 \times 10^{-12}\ N$. The magnetic forces on these particles stayed at $F_{M_{15MP}} = 9.7 \times 10^{-11}\ N$ and $F_{M_{9MP}} = 2.09 \times 10^{-11}\ N$ at all flow rates while the exposure time increased from t=~0.24 s at Q=1.5 mL/hr to t=~1.46 s at Q=0.25 mL/hr, resulting in MPs deflecting towards the sidewall more significantly at lower flow rates. An interesting observation in Fig. 3-3 was the sudden shift of 15 µm MPs to the wall at Q=0.5 mL/hr. In this condition, $\sum(F_L + F_E)_{15MP} = 4.31 \times 10^{-11} N$ was less than $F_{M_{15MP}}$, while at Q=0.75

mL/hr, $\sum(F_L + F_E)_{15MP} = 9.70 \times 10^{-11}N$ which was comparable to the magnetic force. We should also note that in this situation, when decreasing the flow rate from 1.5 to 0.25 mL/hr, the El number remains at 10.75 providing dominant elastic forces on 15 µm NMPs to stay focused at the channel centerline, but the dispersion increases since the magnitude of forces keeping them focused continues to decrease with flow rate reduction.

By changing the PEO concentration in Fig. 3-4, the viscosity and relaxation time of the solution changes which consequently result in changes in the inertial (Eq. 1) and elastic (Eq. 3) forces and hence the El number (Eq. 7). The elastic force is directly proportional to both the relaxation time and the viscosity. Therefore, El number becomes directly proportional to both parameters. Decreasing the PEO concentration from 2000 to 1000 and 500 ppm decreases the Wi number from 12.12 to 7.75 and 4.92 and increases the Re number from 1.13 to 2.01 and 2.57. Accordingly, El number decreases from 10.75 to 3.87 and 1.91 at the corresponding PEO concentrations above. Calculating the forces in these cases shows that for 15 µm MP, the sum of elastic and inertial forces decreased from $3.88 \times 10^{-10}\ N$ to $1.61 \times 10^{-10}\ N$ and $9.62 \times 10^{-11}\ N$, while $F_{M_{15MP}} = 9.7 \times 10^{-11}\ N$. For 9 µm MP, the sum of elastic and inertial forces decreased from $5.03 \times 10^{-11}\ N$ to $2.08 \times 10^{-11}\ N$ and $1.25 \times 10^{-11}\ N$, while $F_{M_{9MP}} = 2.09 \times 10^{-11}\ N$. The decrease in the elastic force and Wi number enhances the ability of the magnetic force to pull the particles closer to the sidewall in the channel, since the elastic force is mainly responsible for keeping the particles at the center. As expected, NMPs always stay under the dominant effect of the elasto-inertial forces and keep focused at the center of the channel since the El number does not get smaller than unity.

Dimensions of the channel affect the inertial and elastic forces as well as *Re*, *Wi*, and *El* numbers according to Eq. 1-4 and 5-7. By decreasing the microchannel size from 90 µm to 70 µm in Fig. 3-5 and for a 2000 ppm PEO solution, *El* number increases from 10.75 to 17.75. *Re* and *Wi*

numbers are also higher for the 70 µm channel at similar flow velocities. This shows that the elastic and inertial forces are more effective in keeping the particles at the center of the smaller channel. For instance, at the flow rate of 0.5 mL/hr, for the 70 µm channel, $\sum(F_L + F_E)_{15MP} = 3.11 \times 10^{-10}N$ and $\sum(F_L + F_E)_{9MP} = 4.03 \times 10^{-11}N$, which were an order of magnitude higher than similar forces in the 90 µm channel and the magnetic forces on the corresponding MPs. Although, the El number increased in the 70 µm microchannel, it was still not high enough for the NMPs to show pure viscoelastic focusing (at 4 channel corners in addition to the center) and they stayed elasto-inertially focused at the center at all flow rates.

It can be concluded from Fig. 3-6 that the hydrodynamic forces can be neglected in the expansion zone as the positions of particles were not a function of the expansion angle. Yet, the dispersion of particles could slightly be controlled by finding the best angle of the expansion channel. In our case, the device with a 45 degrees expansion zone showed the lowest dispersion of particles.

Chapter 4

PARTICLE AND BACTERIA SORTING USING THE MICROFLUIDIC INERTIO-MAGNETO-ELASTIC TECHNIQUE

Based on the literature reviewed in Chapter 1, it was determined that there is a gap in the field of microfluidics for performing high-throughput, sheathless, and multiplex (more than 2 substances) separation of particles and biological analytes in viscoelastic fluids. We aimed for reaching this goal by modifying and enhancing the inertia-magnetic separation method in our group[71]. Therefore, in Chapter 3, we conducted a parametric study to acquire a better understanding of the inertia-elastic focusing and inertia-elasto-magnetic deflection of magnetic and non-magnetic particles in our device.

In this chapter, we have used the insights from the previous chapters to select and test recipes in which three microparticles (9 and 15 µm MP and 15 µm NMP) in viscoelastic PEO solutions can be separated from each other with high purity and efficiency (Section 4.1). We have also demonstrated the application of our device in biological sample preparation by showing the separation of two bacteria-tagged particles as a proof-of-concept (Section 4.2).

4.1 TRIPLEX INERTIA-MAGNETO-ELASTIC (TIME) SORTING OF MICROPARTICLES

Based on the experimental results obtained in Chapter 3, we identified two recipes in which TIME sorting of 9 µm MP, 15 µm MP, and 15 µm NMP in viscoelastic fluids could be achieved with the highest possible efficiencies. These recipes included a magnetic field strength of 200 mT and a flow rate of 1.5 mL/hr, while using a 25 mm-long magnet for the 2000 ppm PEO solution (Recipe 1) and a 12.5 mm-long magnet for the 1000 ppm PEO solution (Recipe 2). The expected performance of these recipes can be seen in Fig. 3-1 and Fig. 3-4. To verify our hypothesis, triplex experiments were conducted in three trials and the number of particles flowing through the mini-outlet channels 1-21 at the end of the expansion channel (Fig. 2-1c) was counted in maximum 10 s intervals. Normalized results are shown in Fig. 4-1 showing that triplex particle sorting in viscoelastic fluids could be achieved with our device.

As expected from singleplex experiments, triplex sorting was achieved for both recipes in Fig. 4-1. This is because 9 µm MPs were under the dominant effect of magnetic forces and pulled towards the channel sidewall while 15 µm NMP only experienced elasto-inertial forces and focused in the center of the channel. The 15 µm MPs experienced magnetic and elasto-inertial forces and assumed positions in the middle of the channel.

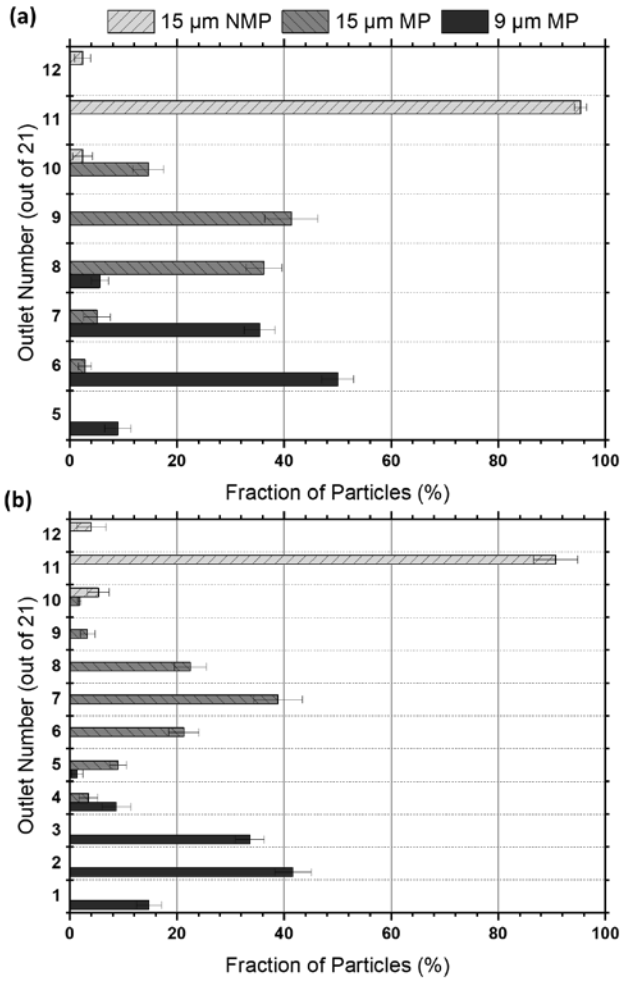

Figure 4-1 Fraction of 9 µm MP, 15 µm MP, and 15 µm NMP counted at each mini-outlet channel, with (a) Recipe 1: 200 mT, 25 mm magnet at 1.5 mL/hr for 2000 ppm PEO-water solution, and (b) Recipe 2: 200 mT, 12.5 mm magnet at 1.5 mL/hr for 1000 PEO-water solution.

As discussed in Chapter 2, the efficiency and purity of sorting for each particle were calculated in outlets where they were dominant in number. Accordingly, in Recipe 1 (Fig. 4-1a), outlets 5-7 were selected for 9 µm MP, outlets 8-10 for 15 µm MP, and outlets 11-12 for 15 µm NMP. In Recipe 2 (Fig. 4-1b), outlets 1-4 were selected for 9 µm MP, outlets 5-9 for 15 µm MP, and outlets 10-12 for 15 µm MP. Microfluidic devices can be fabricated with high resolution and precision, hence, positioning reservoirs to collect the sorted particles in the outlets above is not a significant challenge in future applications. The obtained efficiency and purity values for both recipes are reported in Table 2, with Recipe 2 yielding a slightly better performance than Recipe 1. In Recipe

2, particles are separated across 12 mini-outlets, while in Recipe 1, particle separation takes place across 8 mini-outlets. These novel results demonstrate that our technique can be used for triplex sorting of microparticles in viscoelastic fluids with >92% efficiency and purity.

Table 2. Efficiency and purity of TIME sorting of microparticles

	Recipe 1 (Fig. 4-1a)			**Recipe 2 (Fig. 4-1b)**		
Particle	**9 µm MP**	**15 µm MP**	**15 µm NMP**	**9 µm MP**	**15 µm MP**	**15 µm NMP**
Efficiency (%)	94.4 ± 1.6	92.2 ± 1.6	97.7 ± 1.9	98.6 ± 1.1	94.8 ± 1.5	100
Purity (%)	92.4 ± 1.4	92.1 ± 0.6	100	96.6 ± 1.7	98.6 ± 1	98.3 ± 0.3

4.2 DUPLEX INERTIA-MAGNETO-ELASTIC (DIME) SORTING OF BACTERIA

In the first chapter, we discussed that one of the most important applications of microfluidic particle sorting is in separation of cells like circulating tumor cells, microorganisms like bacteria and molecules like proteins and DNA from complex fluids. It has been shown that cells or bacteria can either be used as non-magnetic particles or attached to magnetic or non-magnetic micro- and nano-particles for manipulation in microfluidic sorting devices. In the latter method, particles can act as carriers for the cells or bacteria while adding various properties to the conjugated assembly that may be necessary for specific separation, such as attaining magnetic properties or a larger size.

In order to demonstrate the application of our method, i.e. inertia-magneto-elastic separation, in biological sample preparation, we designed and fabricated a device with three outlets as discussed in Chapter 2. In this device, waste solution and non-target microorganisms can be ejected from the top outlet while the other two outlets can be used for separation and extraction of two target substances such as the two different particle-bacteria conjugates used in our study. One of the most

convenient possibilities was to use one magnetic and one non-magnetic particle. Each of these particles could be first attached to a bacterium strain, then mixed together at different concentrations and tested in the device.

We needed to choose two bacteria strains which could be distinguished from each other after culturing, but still similar enough to show affinity towards the same antibody for a simpler sample preparation process. Therefore, we chose the *E. coli* K-12 JM83 and *E. coli* BL21 strains which will be called JM83 and BL21 for simplicity in the following text. These strains were ideal for our application due to various reasons. We could use the same type of antibody to conjugate these bacteria to microparticles because of the similarities between the K and B strains. Moreover, their cultured colonies on MacConkey Agar plates show different colors and are distinguishable from each other, where JM83 turns out as white colonies and BL21 turns out as purple colonies (Fig. 4-2). Lastly, the JM83 strain has antibiotic resistance to Streptomycin which can be used as an additional asset in measuring the concentration of JM83 in mixed samples simply by dosing the agar plates with the antibiotic to prevent the BL21 strain from growing.

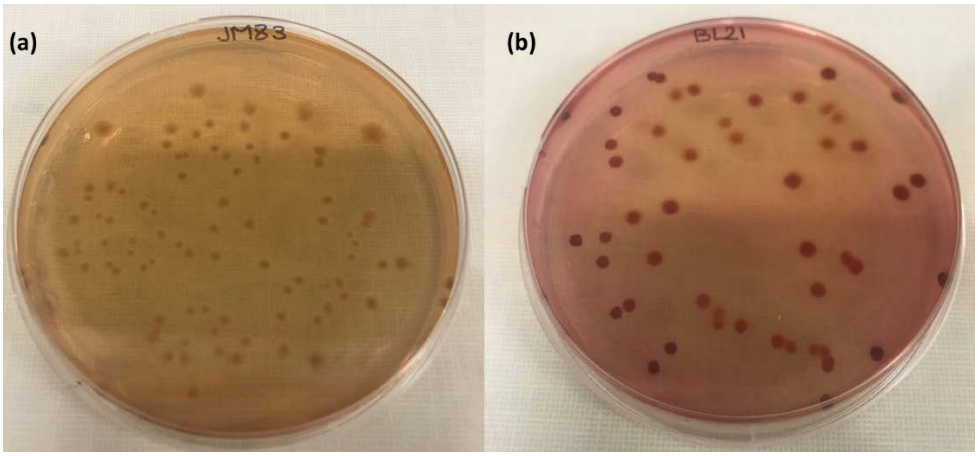

Figure 4-2 Colonies formed on MacConkey plates from (a) E. coli K12 JM83 with white color and (b) *E. coli* BL21 with purple color.

As expected from the results of TIME separation in Fig. 4-1(a-b), 9 µm MP and 15 µm NMP do not have any interference and the purity and efficiency of 100% is achievable in this case. Therefore, we chose the 9 µm MP as a carrier for JM83 and the 15 µm NMP as a carrier for BL21. We expected the 15µm NMP-BL21 conjugates to exit from the middle outlet and the 9 µm MP-JM83 conjugates to exit from the lower outlet. In the sections below, we report our results for conjugating bacteria to microparticles first (section 4.2.1) and their subsequent sorting in our device (section 4.2.2).

4.2.1 Immunological Conjugation of Bacteria to Microparticles

To attach the bacteria to the particles, two different biological bonds where used. First, the strong binding between two proteins called Streptavidin and Biotin where used to attach biotinylated antibodies to the commercially available Streptavidin-coated particles. Bacteria were then attached to the antibody-coated particles due to the specific affinity-based binding between bacteria's antigens and the antibodies on the particles. Details of the sample preparation process were explained in Chapter 2 and Appendix A. A schematic of the binding sequence can be seen in Figure 4-3.

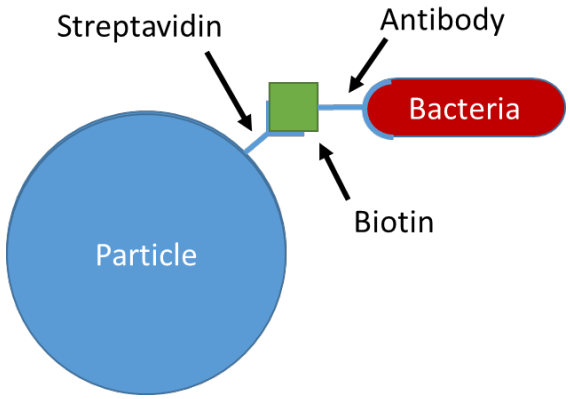

Figure 4-3 Schematic of the affinity-based attachment of Streptavidin-coated particle to bacteria

We characterized the bacteria-particle conjugation process based on three parameters. The first parameter was the concentration of source bacteria, which could be measured by culturing a serially diluted sample of the source stock (overnight culture) before adding it to the particle solution for conjugation. The second parameter approximated the concentration of the unattached bacteria right after incubation with particles, which could be measured by culturing a serially diluted sample of the supernatant after the first wash of the particle-bacteria cocktail. Finally, a diluted sample of the particle-bacteria solution was cultured to find the concentration of the attached bacteria as the third parameter.

Ideally, the sum of attached and unattached bacteria should be equal to the input bacteria if each particle only attaches to one bacterium. To investigate this expectation for particle-to-bacteria ratios in the orders of 0.01, 1, and 100, we examined the conjugation yield defined as the ratio of the attached bacteria concentration to the input bacteria concentration. We also calculated the recovery rate as the ratio of the sum of attached and unattached bacteria to the input bacteria. These results for 9 µm MP-JM83 and 15 µm NMP-BL21 conjugation are shown in Table 3.

Table 3. Bacteria-microparticle conjugation yields at three different bacteria to particle ratios of 100, 1 and 0.01.

Particle[1]-to-Bacteria[2] ratio (order)	**Bacteria**	**Input (CFU/ml)**	**Unattached (CFU/ml)**	**Attached (CFU/ml)**	**Conjugation Yield (%)**	**Recovery Rate (%)**
0.01	**JM83**	8.8×10^9	6.6×10^9	1.9×10^7	0.2	75.2
	BL21	5.7×10^8	4.4×10^8	2.7×10^6	0.5	77.7
1	**JM83**	7.8×10^7	6.1×10^7	1.1×10^7	14.1	92.3
	BL21	4.8×10^6	2.4×10^6	1.9×10^6	39.6	89.6
100	**JM83**	6.3×10^5	2.2×10^4	5.5×10^5	87.3	90.8
	BL21	5×10^4	1.4×10^3	4.7×10^4	94.0	96.8

[1] Particles used were 9 µm MP and 15 µm NMP
[2] Bacteria used were *E. coli* K12 JM83 and *E. coli* BL21 strains

By examining the conjugation yield values in Table 3, we can see that in cases where the bacteria outnumber the particles, we have the lowest yields, where less than 1% of the bacteria attach to the particles. However, in these cases we have the highest raw number of the attached bacteria due to the high concentration of source bacteria. By increasing the particle-to-bacteria ratio, it can be seen that the number of attached bacteria decreases but on the other hand, higher fractions of the bacteria attach to the particles. This continues to the point that up to 94% of the input bacteria can be attached to the target particles for cases where there are more than a hundred particles for each bacterium.

There are multiple steps of centrifugation and washing involved in preparation of bacteria-particle conjugate samples. Losing bacteria during these steps is inevitable which in our experiments can be evaluated by the recovery rates reported in Table 3. As shown, for the cases where the number of bacteria were dominant in the sample, the recovery rate was as high as 77.7%. However, decreasing the number of bacteria to the same order of magnitude as the particles, and even 100 times lower, resulted in an increase in the recovery rate up to 96.8%.

It can be concluded from the results that there is around 10% error in the conjugation and counting process. This error can increase to around 25% where the bacteria outnumbers the particles. Both the recovery and conjugation rates increase by having more particles than bacteria, which implies that the chances of particle-bacteria collision and conjugation increases by having each bacterium surrounded by lots of particles. However, this does not imply that having a large number of bacteria is not beneficial, as we have the largest number of attached bacteria in cases with high bacteria to particle ratio. Therefore, to have more attached bacteria, we need to increase the concentration of input bacteria, but to lose fewer bacteria in the process, for example in cases where the target is

rare, we need to increase the number of particles, to ensure the highest conjugation yield is achieved.

Various reasons can be attributed to the observed error. Among those, we speculate that the handling error during the wash steps and immobilization is the most important one. Some unattached bacteria can be immobilized alongside the particles during magnetic separation or centrifugation which decreases the concentration of supernatant and results in a decrease in the number of unattached bacteria. Another important source of error is the accuracy of serial dilution and CFU counting as the counting method, since it assumes completely homogeneous solution at every dilution step. However, there is always a chance of missing some bacteria especially where the sample gets more diluted.

4.2.2 DIME Sorting of Bacteria

The particle-conjugated bacteria in the previous section were used to demonstrate the application of inertia-magneto-elastic sorting method in duplex bacteria separation. We aimed to investigate the effects of particle-to-bacteria ratio and input conjugate concentration on the separation performance. Although the former parameter attributes to the input conjugate concentration, it leads to various ratios of unconjugated particles in the sample that we wanted to investigate independently. Mixed solutions of 9 μm MP-JM83 and 15 μm NMP-BL21 conjugates were prepared, at three bacteria-to-particle ratios and three conjugate concentrations, in 2000 ppm PEO-PBS solutions with a total sample volume of 2 mL. Samples were tested in the device with three outlets using Recipe 1 reported in Figure 4-1. The first solution was prepared from mixing the conjugates at the same concentrations reported in Table 3. The second and third solutions were prepared by diluting the first solution to ~0.1x and ~0.01x, respectively. The collected samples

from each outlet were cultured on MacConkey plates with and without antibiotic Streptomycin. In cases where we did not expect particles to exit from an outlet (e.g., the upper outlet for both particles and the middle outlet for 9 μm MP-JM83), samples were cultured with two orders of magnitude higher concentration to achieve a 1% accuracy in determining the number of bacteria conjugates. The concentration of bacteria collected from each outlet was measured and reported in Fig. 4-4.

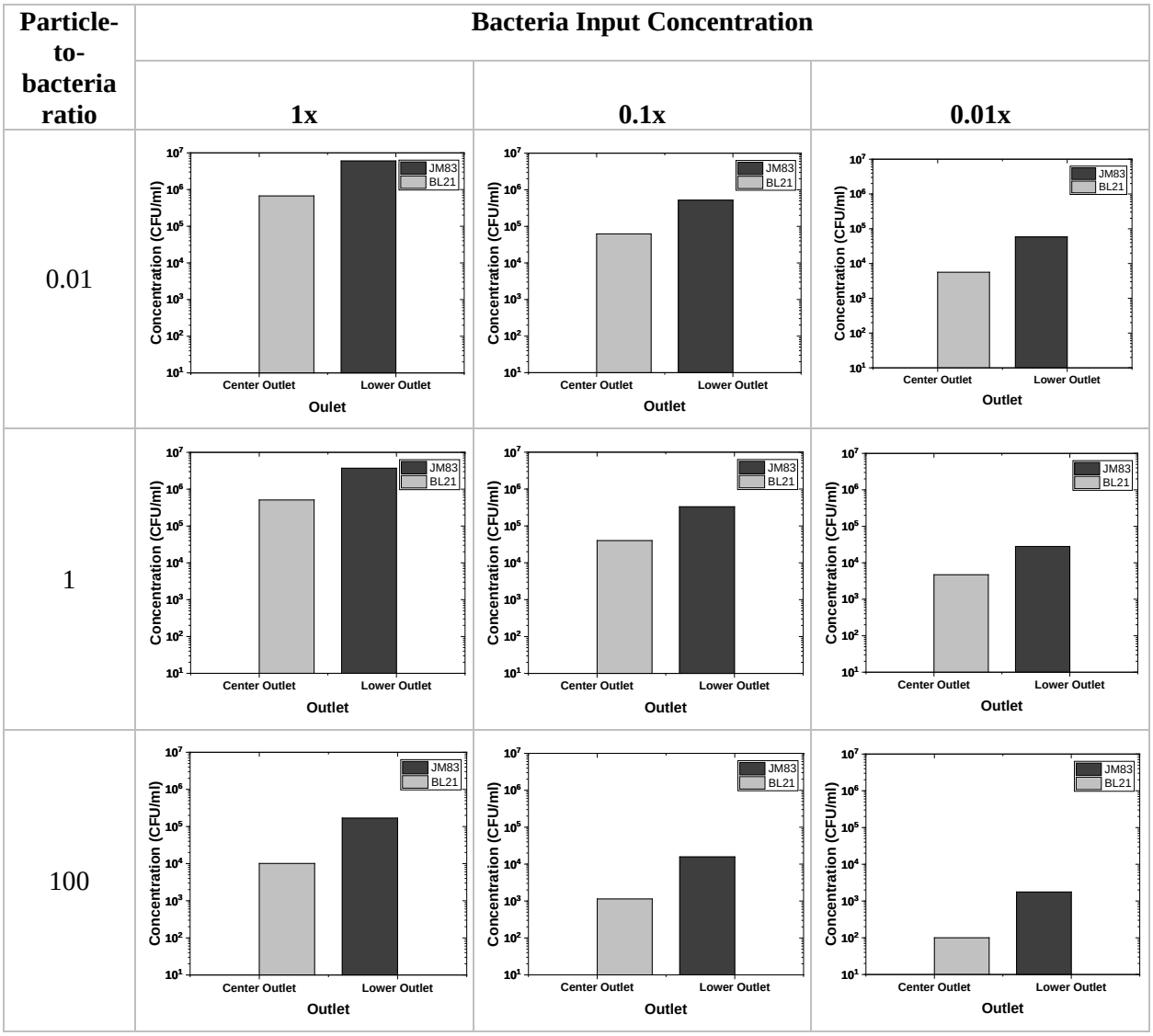

Figure 4-4 Concentration of collected bacteria from two outlets at three input concentrations. Three bacteria to particle conjugation ratios were tested. The upper outlet is not shown as it did not contain any bacteria (<1% impurity)

The results shown in Fig. 4-4 clearly indicate that in each scenario, the majority of JM83 bacteria were collected from the lower outlet while the concentration of BL21 bacteria was dominant in the central outlet of the device. This was consistent with the sorting results obtained in Chapter 3 for particles, demonstrating that the separation phenomena governing the particles also apply to the bacteria-particle conjugates in our device. We did not detect any bacteria in the upper outlet of the device. Accordingly, the efficiency and purity of duplex bacteria sorting using the elasto-inertia-magnetic technique were determined to be higher than 99%. It can be also seen in Fig. 4-4 that in all three particle-to-bacteria ratio cases, by diluting the input sample by 1-2 orders of magnitude, the absolute concentration of the collected bacteria conjugates decreases by the same order of magnitude while keeping the sorting efficiencies and purities at very high levels. All in all, we concluded that the particle-to-bacteria ratio and the input conjugate concentration had no significant impact on the sorting efficiency and purity in our device.

A performance parameter that is widely neglected in the microfluidics sorting literature is the recovery rate. It can be calculated by dividing the concentration of the collected conjugates to the concentration of the same bacteria in the input mixed sample. The recovery rates for the nine cases in Fig. 4-4 are reported in Table. 4 and the averaged values for three input concentration scenarios are presented in Fig. 4-5.

Table 4. Recovery Rates of the DIME separation device at different input concentrations and bacteria-to-particle ratios

Particle-to-bacteria ratio	**Bacteria Input Concentration**					
	1x		**0.1x**		**0.01x**	
	JM83	**BL21**	**JM83**	**BL21**	**JM83**	**BL21**
0.01	70%	55%	68%	57%	75%	51%
1	74%	60%	67%	52%	63%	61%
100	68%	52%	63%	64%	71%	57%

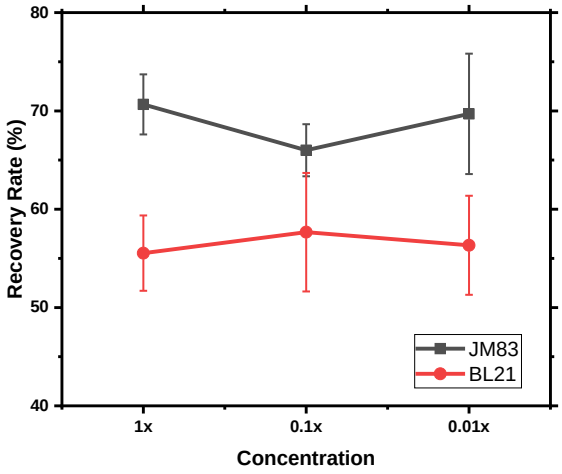

Figure 4-5 Average recovery rate of JM83 and BL21 bacteria at three input concentrations tested with Recipe 2 in the device.

The recovery rate of BL21 bacteria which were attached to the 15 µm NMP is generally lower than the JM83 bacteria which were attached to the 9 µm MP. One of the main reasons for this can be the higher weight of the 15 µm NMP which causes them to sediment inside the syringe and the channel preventing them from entering and exiting the channel, respectively. This effect can be minimized by using smaller particles or shaking the syringe frequently to reduce the sedimentation. The standard deviation for the lowest concentration level is also higher than the other two cases. In this case, we were dealing with a much lower number of particles which may cause some inconsistencies in terms of processing and manipulating the samples. Overall, the recovery rate results were consistent and did not show major dependency on the concentration of particles flowing into the device.

Chapter 5
Thesis Summary and Future Work

5.1 THESIS SUMMARY

Sample preparation is an important step in biological testing of food and water at the Point-of-Use (PoU). Currently, the sample preparation steps usually occur off-chip, which requires lab equipment and is costly in terms of time and needed labor. Therefore, there is a need to perform sample preparation on the chip which would be faster, cheaper, and easier. One of the needed processes in many sample preparation applications is multiplex separation of biological analytes in viscoelastic fluids such as blood, DNA solutions and milk.

In this thesis, we have developed a technique to perform inertia-elasto-magnetic separation of magnetic (MPs) and non-magnetic (NMPs) particles as surrogates and or affinity-based conjugates for target biological analytes. We first conducted a parametric study on the focusing and deflection of MPs and NMPs in the presence of inertial, elastic, and magnetic forces in a microchannel with a permanent magnet beside it. In our microfluidic device, MPs and NMPs first focus at the center of the straight square microchannel, due to the combined effects of the elastic and inertial forces. At the end of the channel, the MPs are pulled to the sidewall where the permanent magnet is

positioned before they are released into an expanded channel for imaging and ejection from the device. The elastic, inertial, and magnetic forces highly depend on the particle size and their magnetic characteristics. Therefore, MPs take different equilibrium positions based on their sizes as they get deflected in the microchannel. The effect of magnetic field exposure length, magnetic field strength, flow rate, fluid viscoelasticity, channel size, and expansion angle were studied on the focusing, deflection, and dispersion of the particles. It was shown that by increasing the magnetic field strength, magnet length and channel size and decreasing the flow rate and viscoelasticity of the fluid, particles deflect more toward the magnet due to the dominance of magnetic force over the inertial and elastic forces.

Based on the results obtained in the parametric study, recipes were selected to perform Triplex Inertia-Magneto-Elastic (TIME) sorting of particles in viscoelastic fluids. Using these recipes, separation of 9 µm and 15 µm MPs and 15 µm NMPs was achieved with a minimum purity and efficiency of 92%.

Finally, a device with three outlets was designed and fabricated to separate two bacteria strains, i.e. *E. coli* K12 JM83 and *E. coli* BL21, attached to MPs and NMPs and spiked into PEO solutions. Minimum bacteria separation purity and efficiency of 99% was achieved. The findings of bacteria and microparticle sorting demonstrate the potential of our device to be used as an on-chip sample preparation tool at the PoU, capable of separating up to three analytes from each other in viscoelastic fluids.

5.2 FUTURE WORK

Continuing this project, the following ideas and suggestions are recommended for further investigation.

Based on the TIME particle sorting results, a device can be designed and fabricated with multiple outlets to perform separation of particles, cells and bacteria. In this device, large cells like red blood cells can act as the non-target non-magnetic particles and be separated from two different magnetically-labelled target bacteria. DIME separation of bacteria can also be tested for various applications such as separating a cell from a bacteria strain, by replacing the NMP with a cell. However, the target cell should be large enough to get focused inside the channel.

One of the areas in which the performance of TIME and DIME devices can be enhanced is increasing the recovery rate of the particles. As stated at the end of Chapter 4, the main reason for the relatively low recovery rate of the particles is sedimentation inside the syringe and at the outlets. As a recommendation for enhancing the performance in real applications at the PoU, sedimentation inside the syringe can possibly be minimized by using a portable syringe pump and placing it on a shaker or using a small electrical vibrator attached to the syringe. The sedimentation at the outlets can be eliminated by placing the device downwards so that the gravity can help collecting the particles.

The parametric study can be continued by performing a more thorough theoretical study which may include analytical and numerical investigations. This may result in finding an empirical equation for calculating the deflection position of particles, having the experimental parameters as the inputs for verification and validation. This can significantly help designing special devices for custom applications based on the fluid properties and the size of targets that need to be separated.

Our chip can be accompanied by another microfluidic device that takes antibody-coated particles and mixed bacteria solutions as two inputs and delivers the particles attached with target bacteria as the main outlet (moving to TIME device for separation) and unattached bacteria as the waste.

As an alternative application, the TIME separation device can act as a filter which gets particle solution with a wide size dispersion (similar to the 15 μm MP that we used) and divides them into portions with lower dispersion (mono-dispersed particles). As we showed in Chapter 3, elasto-inertially focused magnetic particles deflect due to magnet based on their size, meaning that the wider their size distribution, the higher their dispersion in the expansion region, with smaller particles showing more deflection. This phenomenon can be used for size fractionation of magnetic particles.

Chapter 6
Appendices

Appendix A - LABELING *E. COLI* WITH MAGNETIC AND NON-MAGNETIC MICROPARTICLES

In this section, procedures followed to conjugate specific bacteria to magnetic microparticles is described, consisting of methodologies used for bacteria growth, coating particles with antibodies, labelling bacteria with the microparticles, and counting the attached and unattached bacteria

A1. *E. coli* Growth

1. Using a sterile inoculating loop or toothpick, streak out *E. coli* K12 JM83 and E. coli BL21 onto LB plates

2. Incubate overnight in 37°C incubator.

3. Pick a single colony using sterile loop or toothpick from each plate and inoculate in 3-5mL LB media in culture tubes separately and incubate overnight in 37°C shaking incubator (200-225 RPM).

4. In the meantime, prepare antibody-coated beads as described in “Bead Preparation”

5. Transfer 3 mL culture to 2x 1.5 mL tubes and spin 30 sec at 10,000 RPM (16,000 x g) in microcentrifuge. Remove supernatant and gently resuspend pellet (pipet up/down) in 1 mL PBS+0.1%BSA. *(This step should be done before step 6 of "Cell isolation" part.)*

A2. Bead Preparation

1. Vortex magnetic beads for several seconds and transfer 100 µl beads to a 1.5 mL tube.

    - Spherotech, #SVM-80-5:
        - 9 µm magnetic particles, coated with Streptavidin
        - ~1.75 x 10^7 beads/ml
        - Analyte binding capacity: 206 ng/mg (100 µl 1%) beads (Quick Particle data sheet)

    - Spherotech #SVP-150-4:
        - 15 µm polystyrene particles, coated with Streptavidin
        - ~2.5 x 10^6 beads/ml
        - Analyte binding capacity: 206 ng/mg (100 µl 1%) beads (Quick Particle data sheet)
2. Wash beads with 1 mL PBS+0.1% BSA and invert tube several times.

3. Place tube on magnet for 3 min and carefully remove the supernatant to avoid bead loss.

4. Remove tube from magnet and resuspend in 1 mL 1x PBS+0.1% BSA

5. Repeat wash step, 2 more times.

A3. Cell Isolation – Direct Technique (repeat for each bacteria strain with respective bead size)

1. Add 5 µl Anti-E. coli antibody (Biotin) (4 mg/ml) Abcam (ab20640) to 1 mL washed beads from Step 5 of Bead Prep.

2. Incubate for 30-60 min at room temperature with gentle rotation.

3. Place MP tube on magnet for 3 min (centrifuge NMP tube for 20 seconds with 5000 RPM) and carefully remove and discard supernatant

4. Remove tube and wash beads 4X with 1 mL PBS+0.1% BSA to remove unbound antibodies

5. Place MP tube on magnet for 3 min (centrifuge NMP tube for 20 seconds with 5000 RPM) and carefully remove supernatant
6. Add 1 mL cell suspension (see "Growth of *E. coli*") and resuspend. Save 100 µl of cell suspension as **INPUT**
7. Incubate for 60 min at room temperature with gentle rotation.
8. Place tube on magnet for 3 min and carefully transfer supernatant to fresh tube labelled **UNATTACHED**.
9. Remove tube and wash beads 3X with 1 mL PBS+0.1% BSA to remove unbound cells
10. Resuspend beads in 0.5 mL PEO+PBS+0.1% BSA and plate samples. See "Counting isolated bacteria".

A4. Counting isolated bacteria

1. Aseptically make ten-fold serial dilutions of samples in LB and spread on one MAC plate and one MAC+Strep plate. Proper dilution factor for each sample will be determined by trial and error.

2. Incubate plates over-night at 37C

3. Count the number of bacterial colonies that appear on each plate that has between 30 and 300 colonies.

Any plate which has more than 300 colonies is designated as "too many to count (TMC)". Plates with fewer than 30 colonies do not have enough individuals to be statistically acceptable "too few to count (TFC)".

4. To calculate the estimated number of bacteria on the surface that you tested, use the following formula:

$$B = N/d,$$

where: B = # bacteria; N = average # colonies; d = dilution factor.

Appendix B – CALCULATING THE MAXIMUM FOCUSING LENGTH

In this section, we calculate the maximum inertia-elastic focusing length as a determining parameter in designing the device. The length of the channel before the magnet should be equal or longer than the maximum focusing length that can happen in our device. Del Giudice et al.[77] have experimentally shown that in order to achieve single-point elasto-inertial 3D focusing in a square channel, the non-dimensional number $De\left(\frac{L}{H}\right)\beta^2$ should be equal to 1, where *De* is the Deborah number and equals half of the Weissenberg number (Eq. 6), L is the channel length, H is the channel height, and β is the blockage ratio or the ratio of particle diameter to the channel hydraulic diameter. Therefore, we can define the following equation to find the required channel length for elasto-inertial focusing.

$$L = \frac{H}{De\ \beta^2}$$

From the theory in Chapter 3, we know that the worst case scenario for elasto-inertial focusing is with the smallest particle, lowest flow rate, lowest fluid viscoelasticity, and the largest channel size. This happens with 9 µm MP at the flow rate of 0.25 mL/hr and PEO concentration of 500 ppm, in the 90 µm microchannel. In this case, De equals 0.41, H equals 90 µm and β equals 9 µm/90 µm = 0.1. Therefore, the focusing length can be calculated as 21.97 mm.

References

(1) Lee, W. G.; Kim, Y.-G.; Chung, B. G.; Demirci, U.; Khademhosseini, A. Nano/Microfluidics for Diagnosis of Infectious Diseases in Developing Countries. *Adv. Drug Deliv. Rev.* **2010**, *62* (4–5), 449–457.

(2) Yager, P.; Domingo, G. J.; Gerdes, J. Point-of-Care Diagnostics for Global Health. *Annu. Rev. Biomed. Eng.* **2008**, *10* (1), 107–144.

(3) Majors, C. E.; Smith, C. A.; Natoli, M. E.; Kundrod, K. A.; Richards-Kortum, R. Point-of-Care Diagnostics to Improve Maternal and Neonatal Health in Low-Resource Settings. *Lab Chip* **2017**.

(4) Wu, M. Y.-C.; Hsu, M.-Y.; Chen, S.-J.; Hwang, D.-K.; Yen, T.-H.; Cheng, C.-M. Point-of-Care Detection Devices for Food Safety Monitoring: Proactive Disease Prevention. *Trends Biotechnol.* **2017**, *35* (4), 288–300.

(5) Gubala, V.; Harris, L. F.; Ricco, A. J.; Tan, M. X.; Williams, D. E. Point of Care Diagnostics: Status and Future. *Anal. Chem.* **2012**, *84* (2), 487–515.

(6) Foudeh, A. M.; Fatanat Didar, T.; Veres, T.; Tabrizian, M. Microfluidic Designs and Techniques Using Lab-on-a-Chip Devices for Pathogen Detection for Point-of-Care Diagnostics. *Lab Chip* **2012**, *12* (18), 3249–3266.

(7) Sharma, S.; Zapatero-Rodr??guez, J.; Estrela, P.; O'Kennedy, R. Point-of-Care Diagnostics in Low Resource Settings: Present Status and Future Role of Microfluidics. *Biosensors* **2015**, *5* (3), 577–601.

(8) Nayak, S.; Blumenfeld, N. R.; Laksanasopin, T.; Sia, S. K. Point-of-Care Diagnostics:

Recent Developments in a Connected Age. *Anal. Chem.* **2016**, acs.analchem.6b04630.

(9) Mach, A. J.; Adeyiga, O. B.; Di Carlo, D. Microfluidic Sample Preparation for Diagnostic Cytopathology. *Lab Chip* **2013**, *13* (6), 1011.

(10) Dharmasiri, U.; Witek, M. A.; Adams, A. A.; Soper, S. A. Microsystems for the Capture of Low-Abundance Cells. *Annu. Rev. Anal. Chem.* **2010**, *3* (1), 409–431.

(11) Clark, K. D.; Zhang, C.; Anderson, J. L. Sample Preparation for Bioanalytical and Pharmaceutical Analysis. *Anal. Chem.* **2016**, *88* (23), 11262–11270.

(12) Gervais, L.; De Rooij, N.; Delamarche, E. Microfluidic Chips for Point-of-Care Immunodiagnostics. *Adv. Mater.* **2011**, *23* (24).

(13) Yetisen, A. K.; Akram, M. S.; Lowe, C. R. Paper-Based Microfluidic Point-of-Care Diagnostic Devices. *Lab Chip* **2013**, *13* (12), 2210.

(14) Jung, W.; Han, J.; Choi, J. W.; Ahn, C. H. Point-of-Care Testing (POCT) Diagnostic Systems Using Microfluidic Lab-on-a-Chip Technologies. *Microelectron. Eng.* **2014**, *132*, 46–57.

(15) Mauk, M.; Song, J.; Bau, H. H.; Gross, R.; Bushman, F. D.; Collman, R. G.; Liu, C. Miniaturized Devices for Point of Care Molecular Detection of HIV. *Lab Chip* **2017**, *17* (3), 382–394.

(16) Kim, J.; Johnson, M.; Hill, P.; Gale, B. K. Microfluidic Sample Preparation: Cell Lysis and Nucleic Acid Purification. *Integr. Biol.* **2009**, *1* (10), 574.

(17) Toner, M.; Irimia, D. Blood-on-a-Chip. *Annu. Rev. Biomed. Eng.* **2005**, *7* (1), 77–103.

(18) Cui, F.; Rhee, M.; Singh, A.; Tripathi, A. Microfluidic Sample Preparation for Medical

Diagnostics. *Annu. Rev. Biomed. Eng.* **2015**, *17* (1), 267–286.

(19) Hejazian, M.; Li, W.; Nguyen, N. Lab on a Chip for Continuous-Flow Magnetic Cell Separation. *Lab Chip* **2015**, *15* (4), 959–970.

(20) Mattanovich, D.; Borth, N. Applications of Cell Sorting in Biotechnology. *Microb. Cell Fact.* **2006**, *5*, 12.

(21) Wyatt Shields IV, C.; Reyes, C. D.; López, G. P. Microfluidic Cell Sorting: A Review of the Advances in the Separation of Cells from Debulking to Rare Cell Isolation. *Lab Chip* **2015**, *15* (5), 1230–1249.

(22) Kim, S.; Han, S.-I.; Park, M.-J.; Jeon, C.-W.; Joo, Y.-D.; Choi, I.-H.; Han, K.-H. Circulating Tumor Cell Microseparator Based on Lateral Magnetophoresis and Immunomagnetic Nanobeads. *Anal. Chem.* **2013**, *85* (5), 2779–2786.

(23) Pitt, W. G.; Alizadeh, M.; Husseini, G. A.; McClellan, D. S.; Buchanan, C. M.; Bledsoe, C. G.; Robison, R. A.; Blanco, R.; Roeder, B. L.; Melville, M.; et al. Rapid Separation of Bacteria from Blood???Review and Outlook. *Biotechnol. Prog.* **2016**, *32* (4), 823–839.

(24) Ngamsom, B.; Esfahani, M. M. N.; Phurimsak, C.; Lopez-Martinez, M. J.; Raymond, J. C.; Broyer, P.; Patel, P.; Pamme, N. Multiplex Sorting of Foodborne Pathogens by On-Chip Free-Flow Magnetophoresis. *Anal. Chim. Acta* **2016**, *918*, 69–76.

(25) D'Amico, L.; Ajami, N. J.; Adachi, J. A.; Gascoyne, P.; Petrosino, J. F. Isolation and Concentration of Bacteria from Blood Using Microfluidic Membraneless Dialysis and Dielectrophoresis. *Lab Chip* **2017**, *17*, 1340–1348.

(26) Lim, M. C.; Lee, G. H.; Huynh, D. T. N.; Hong, C. E.; Park, S. Y.; Jung, J. Y.; Park, C. S.;

Ko, S.; Kim, Y. R. Biological Preparation of Highly Effective Immunomagnetic Beads for the Separation, Concentration, and Detection of Pathogenic Bacteria in Milk. *Colloids Surfaces B Biointerfaces* **2016**, *145*, 854–861.

(27) Gossett, D. R.; Weaver, W. M.; MacH, A. J.; Hur, S. C.; Tse, H. T. K.; Lee, W.; Amini, H.; Di Carlo, D. Label-Free Cell Separation and Sorting in Microfluidic Systems. *Anal. Bioanal. Chem.* **2010**, *397* (8), 3249–3267.

(28) Zhu, T.; Cheng, R.; Lee, S. A.; Rajaraman, E.; Eiteman, M. A.; Querec, T. D.; Unger, E. R.; Mao, L. Continuous-Flow Ferrohydrodynamic Sorting of Particles and Cells in Microfluidic Devices. *Microfluid. Nanofluidics* **2012**, *13* (4), 645–654.

(29) Holzner, G.; Stavrakis, S.; deMello, A. Elasto-Inertial Focusing of Mammalian Cells and Bacteria Using Low Molecular, Low Viscosity PEO Solutions. *Anal. Chem.* **2017**, acs.analchem.7b03093.

(30) Faridi, M. A.; Ramachandraiah, H.; Banerjee, I.; Ardabili, S.; Zelenin, S.; Russom, A. Elasto-Inertial Microfluidics for Bacteria Separation from Whole Blood for Sepsis Diagnostics. *J. Nanobiotechnology* **2017**, *15* (1), 3.

(31) Inglis, D. W.; Riehn, R.; Austin, R. H.; Sturm, J. C. Continuous Microfluidic Immunomagnetic Cell Separation. *Appl. Phys. Lett.* **2004**, *85* (21), 5093–5095.

(32) Yassine, O.; Gooneratne, C. P.; Smara, D. A.; Li, F.; Mohammed, H.; Merzaban, J.; Kosel, J. Isolation of Cells for Selective Treatment and Analysis Using a Magnetic Microfluidic Chip. *Biomicrofluidics* **2014**, *8* (3), 1–12.

(33) Qiu, J.; Zhou, Y.; Chen, H.; Lin, J. M. Immunomagnetic Separation and Rapid Detection of

Bacteria Using Bioluminescence and Microfluidics. *Talanta* **2009**, *79* (3), 787–795.

(34) Lee, J.-J.; Jeong, K. J.; Hashimoto, M.; Kwon, A. H.; Rwei, A.; Shankarappa, S. A.; Tsui, J. H.; Kohane, D. S. Synthetic Ligand-Coated Magnetic Nanoparticles for Microfluidic Bacterial Separation from Blood. *Nano Lett.* **2014**, *14* (1), 1–5.

(35) Huang, L. R. Continuous Particle Separation Through Deterministic Lateral Displacement. *Science (80-.).* **2004**, *304* (5673), 987–990.

(36) Yamada, M.; Nakashima, M.; Seki, M. Pinched Flow Fractionation: Continuous Size Separation of Particles Utilizing a Laminar Flow Profile in a Pinched Microchannel. *Anal. Chem.* **2004**, *76* (18), 5465–5471.

(37) Zhang, J.; Yan, S.; Yuan, D.; Alici, G.; Nguyen, N.-T.; Ebrahimi Warkiani, M.; Li, W. Fundamentals and Applications of Inertial Microfluidics: A Review. *Lab Chip* **2016**, *16*, 10–34.

(38) Amini, H.; Lee, W.; Di Carlo, D. Inertial Microfluidic Physics. *Lab Chip* **2014**, *14* (15), 2739–2761.

(39) Zhou, J.; Giridhar, P. V.; Kasper, S.; Papautsky, I. Modulation of Aspect Ratio for Complete Separation in an Inertial Microfluidic Channel. *Lab Chip* **2013**, *13* (10), 1919–1929.

(40) Wang, X.; Liedert, C.; Liedert, R.; Papautsky, I. A Disposable, Roll-to-Roll Hot-Embossed Inertial Microfluidic Device for Size-Based Sorting of Microbeads and Cells. *Lab Chip* **2016**, *16*, 1821–1830.

(41) Wang, X.; Papautsky, I. Size-Based Microfluidic Multimodal Microparticle Sorter. *Lab Chip* **2015**, *15* (5), 1350–1359.

(42) Bhagat, A. A. S.; Kuntaegowdanahalli, S. S.; Papautsky, I. Continuous Particle Separation in Spiral Microchannels Using Dean Flows and Differential Migration. *Lab Chip* **2008**, *8* (11), 1906–1914.

(43) Kuntaegowdanahalli, S. S.; Bhagat, A. A. S.; Kumar, G.; Papautsky, I. Inertial Microfluidics for Continuous Particle Separation in Spiral Microchannels. *Lab Chip* **2009**, *9* (20), 2973.

(44) McGrath, J.; Jimenez, M.; Bridle, H. Deterministic Lateral Displacement for Particle Separation: A Review. *Lab Chip* **2014**, *14* (21), 4139–4158.

(45) Davis, J. A.; Inglis, D. W.; Morton, K. J.; Lawrence, D. A.; Huang, L. R.; Chou, S. Y.; Sturm, J. C.; Austin, R. H. Deterministic Hydrodynamics: Taking Blood Apart. *Proc. Natl. Acad. Sci.* **2006**, *103* (40), 14779–14784.

(46) Beech, J. P.; Jönsson, P.; Tegenfeldt, J. O. Tipping the Balance of Deterministic Lateral Displacement Devices Using Dielectrophoresis. *Lab Chip* **2009**, *9* (18), 2698–2706.

(47) Vig, A. L.; Kristensen, A. Separation Enhancement in Pinched Flow Fractionation. *Appl. Phys. Lett.* **2008**, *93* (20), 203507.

(48) Bhagat, A. A. S.; Kuntaegowdanahalli, S. S.; Papautsky, I. Inertial Microfluidics for Continuous Particle Filtration and Extraction. *Microfluid. Nanofluidics* **2009**, *7* (2), 217–226.

(49) Di Carlo, D. Inertial Microfluidics. *Lab Chip* **2009**, *9* (21), 3038.

(50) Martel, J. M.; Toner, M. Inertial Focusing in Microfluidics. *Annu. Rev. Biomed. Eng.* **2014**, *16*, 371–396.

(51) Zhou, J.; Papautsky, I. Fundamentals of Inertial Focusing in Microchannels. *Lab Chip* **2013**,

13 (6), 1121–1132.

(52) Sarkar, A.; Hou, H. W.; Mahan, A. E.; Han, J.; Alter, G. Multiplexed Affinity-Based Separation of Proteins and Cells Using Inertial Microfluidics. *Sci. Rep.* **2016**, *6*, 23589.

(53) Nivedita, N.; Ligrani, P.; Papautsky, I. Dean Flow Dynamics in Low-Aspect Ratio Spiral Microchannels. *Sci. Rep.* **2017**, *7* (October 2016), 44072.

(54) Fiedler, S.; Shirley, S. G.; Schnelle, T.; Fuhr, G. Dielectrophoretic Sorting of Particles and Cells in a Microsystem. *Anal. Chem.* **1998**, *70* (9), 1909–1915.

(55) Ren, L.; Chen, Y.; Li, P.; Mao, Z.; Huang, P.-H.; Rufo, J.; Guo, F.; Wang, L.; McCoy, J. P.; Levine, S. J.; et al. A High-Throughput Acoustic Cell Sorter. *Lab Chip* **2015**, *15* (19), 3870–3879.

(56) Sang, B. K.; Sang, Y. Y.; Hyung, J. S.; Sang, S. K. Cross-Type Optical Particle Separation in a Microchannel. *Anal. Chem.* **2008**, *80* (7), 2628–2630.

(57) Hejazian, M.; Li, W.; Nguyen, N.-T. Lab on a Chip for Continuous-Flow Magnetic Cell Separation. *Lab Chip* **2015**, *15* (4), 959–970.

(58) Adams, J. D.; Kim, U.; Soh, H. T. Multitarget Magnetic Activated Cell Sorter. *Proc. Natl. Acad. Sci.* **2008**, *105* (47), 18165–18170.

(59) Golozar, M.; Molki, M.; Darabi, J. Computational and Performance Analysis of a Continuous Magnetophoretic Bioseparation Chip with Alternating Magnetic Fields. *Microfluid. Nanofluidics* **2017**, *21* (4), 73.

(60) Phurimsak, C.; Tarn, M. D.; Peyman, S. a; Greenman, J.; Pamme, N. On-Chip Determination of C - Reactive Protein Using Magnetic Particles in Continuous Flow. *Anal.*

Chem. **2014**, *86*, 10552–10559.

(61) Pamme, N.; Manz, A. On-Chip Free-Flow Magnetophoresis: Continuous Flow Separation of Magnetic Particles and Agglomerates. *Anal. Chem.* **2004**, *76* (24), 7250–7256.

(62) Pamme, N. Magnetism and Microfluidics. *Lab Chip* **2006**, *6* (1), 24–38.

(63) Alnaimat, F.; Dagher, S.; Mathew, B.; Hilal-Alnqbi, A.; Khashan, S. Microfluidics Based Magnetophoresis: A Review. *Chem. Rec.* **2018**, 1–18.

(64) Xia, N.; Hunt, T. P.; Mayers, B. T.; Alsberg, E.; Whitesides, G. M.; Westervelt, R. M.; Ingber, D. E. Combined Microfluidic-Micromagnetic Separation of Living Cells in Continuous Flow. *Biomed. Microdevices* **2006**, *8* (4), 299–308.

(65) Bhuvanendran Nair Gourikutty, S.; Chang, C. P.; Puiu, P. D. Microfluidic Immunomagnetic Cell Separation from Whole Blood. *J. Chromatogr. B Anal. Technol. Biomed. Life Sci.* **2016**, *1011*, 77–88.

(66) Miltenyi, S.; Müller, W.; Weichel, W.; Radbruch, A. High Gradient Magnetic Cell Separation with MACS. *Cytometry* **1990**, *11* (2), 231–238.

(67) Pamme, N.; Eijkel, J. C. T.; Manz, A. On-Chip Free-Flow Magnetophoresis: Separation and Detection of Mixtures of Magnetic Particles in Continuous Flow. *J. Magn. Magn. Mater.* **2006**, *307* (2), 237–244.

(68) Tarn, M. D.; Peyman, S. A.; Robert, D.; Iles, A.; Wilhelm, C.; Pamme, N. The Importance of Particle Type Selection and Temperature Control for On-Chip Free-Flow Magnetophoresis. *J. Magn. Magn. Mater.* **2009**, *321* (24), 4115–4122.

(69) Pamme, N.; Wilhelm, C. Continuous Sorting of Magnetic Cells via On-Chip Free-Flow

Magnetophoresis. *Lab Chip* **2006**, *6* (8), 974–980.

(70) Østergaard, S.; Blankenstein, G.; Dirac, H.; Leistiko, O. A Novel Approach to the Automation of Clinical Chemistry by Controlled Manipulation of Magnetic Particles. *J. Magn. Magn. Mater.* **1999**, *194* (1–3), 156–162.

(71) Kumar, V.; Rezai, P. Multiplex Inertio-Magnetic Fractionation (MIMF) of Magnetic and Non-Magnetic Microparticles in a Microfluidic Device. *Microfluid. Nanofluidics* **2017**, *21* (5), 83.

(72) Kumar, V.; Rezai, P. Magneto-Hydrodynamic Fractionation (MHF) for Continuous and Sheathless Sorting of High-Concentration Paramagnetic Microparticles. *Biomed. Microdevices* **2017**, *19* (2).

(73) Hejazian, M.; Phan, D.-T.; Nguyen, N.-T. Mass Transport Improvement in Microscale Using Diluted Ferrofluid and a Non-Uniform Magnetic Field. *RSC Adv.* **2016**, 62439–62444.

(74) Zhu, T.; Marrero, F.; Mao, L. Continuous Separation of Non-Magnetic Particles inside Ferrofluids. *Microfluid. Nanofluidics* **2010**, *9* (4–5), 1003–1009.

(75) Zeng, J.; Deng, Y.; Vedantam, P.; Tzeng, T. R.; Xuan, X. Magnetic Separation of Particles and Cells in Ferrofluid Flow through a Straight Microchannel Using Two Offset Magnets. *J. Magn. Magn. Mater.* **2013**, *346*, 118–123.

(76) Lu, X.; Liu, C.; Hu, G.; Xuan, X. Particle Manipulations in Non-Newtonian Microfluidics: A Review. *J. Colloid Interface Sci.* **2017**, *500*, 182–201.

(77) Del Giudice, F.; Romeo, G.; D'Avino, G.; Greco, F.; Netti, P. A.; Maffettone, P. L. Particle

Alignment in a Viscoelastic Liquid Flowing in a Square-Shaped Microchannel. *Lab Chip* **2013**, *13* (21), 4263.

(78) Lee, D. J.; Brenner, H.; Youn, J. R.; Song, Y. S. Multiplex Particle Focusing via Hydrodynamic Force in Viscoelastic Fluids. *Sci. Rep.* **2013**, *3*, 3258.

(79) Li, D.; Lu, X.; Xuan, X. Viscoelastic Separation of Particles by Size in Straight Rectangular Microchannels: A Parametric Study for a Refined Understanding. *Anal. Chem.* **2016**, *88* (24), 12303–12309.

(80) Lu, X.; Xuan, X. Continuous Microfluidic Particle Separation via Elasto-Inertial Pinched Flow Fractionation. *Anal. Chem.* **2015**, *87* (12), 6389–6396.

(81) Lim, H.; Nam, J.; Shin, S. Lateral Migration of Particles Suspended in Viscoelastic Fluids in a Microchannel Flow. *Microfluid. Nanofluidics* **2014**, *17* (4), 683–692.

(82) Lim, E. J.; Ober, T. J.; Edd, J. F.; Desai, S. P.; Neal, D.; Bong, K. W.; Doyle, P. S.; McKinley, G. H.; Toner, M. Inertio-Elastic Focusing of Bioparticles in Microchannels at High Throughput. *Nat. Commun.* **2014**, *5* (May), 4120.

(83) D'Avino, G.; Maffettone, P. L.; Greco, F.; Hulsen, M. A. Viscoelasticity-Induced Migration of a Rigid Sphere in Confined Shear Flow. *J. Nonnewton. Fluid Mech.* **2010**, *165* (9–10), 466–474.

(84) Yang, S.; Kim, J. Y.; Lee, S. J.; Lee, S. S.; Kim, J. M. Sheathless Elasto-Inertial Particle Focusing and Continuous Separation in a Straight Rectangular Microchannel. *Lab Chip* **2011**, *11* (2), 266–273.

(85) Li, Y.; Zhang, H.; Li, Y.; Li, X.; Wu, J.; Qian, S.; Li, F. Dynamic Control of Particle

Separation in Deterministic Lateral Displacement Separator with Viscoelastic Fluids. *Sci. Rep.* **2018**, *8* (1), 1–9.

(86) Nam, J.; Tan, J. K. S.; Khoo, B. L.; Namgung, B.; Leo, H. L.; Lim, C. T.; Kim, S. Hybrid Capillary-Inserted Microfluidic Device for Sheathless Particle Focusing and Separation in Viscoelastic Flow. *Biomicrofluidics* **2015**, *9* (064117), 1–9.

(87) Del Giudice, F.; Madadi, H.; Villone, M. M.; D'Avino, G.; Cusano, A. M.; Vecchione, R.; Ventre, M.; Maffettone, P. L.; Netti, P. a. Magnetophoresis 'Meets' Viscoelasticity: Deterministic Separation of Magnetic Particles in a Modular Microfluidic Device. *Lab Chip* **2015**, *15*, 1912–1922.

(88) Zhang, J.; Yan, S.; Yuan, D.; Zhao, Q.; Tan, S. H.; Nguyen, N.-T.; Li, W. A Novel Viscoelastic-Based Ferrofluid for Continuous Sheathless Microfluidic Separation of Nonmagnetic Microparticles. *Lab Chip* **2016**, *16*, 3947–3956.

(89) Kim, M. J.; Lee, D. J.; Youn, J. R.; Song, Y. S. Two Step Label Free Particle Separation in a Microfluidic System Using Elasto-Inertial Focusing and Magnetophoresis. *RSC Adv.* **2016**, *6*, 32090–32097.

(90) Kim, M. J.; Lee, D. J.; Youn, J. R.; Song, Y. S. Two Step Label Free Particle Separation in a Microfluidic System Using Elasto-Inertial Focusing and Magnetophoresis. *RSC Adv.* **2016**, *6* (38), 32090–32097.

(91) Yuan, D.; Zhao, Q.; Yan, S.; Tang, S.-Y.; ALICI, G.; Zhang, J.; Li, W. Recent Progress of Particle Migration in Viscoelastic Fluid. *Lab Chip* **2018**, No. ii.

(92) Lu, X.; Liu, C.; Hu, G.; Xuan, X. Particle Manipulations in Non-Newtonian Microfluidics:

A Review. *J. Colloid Interface Sci.* **2017**, *500*, 182–201.

(93) Seo, K. W.; Kang, Y. J.; Lee, S. J. Lateral Migration and Focusing of Microspheres in a Microchannel Flow of Viscoelastic Fluids. *Phys. Fluids* **2014**, *26* (6), 063301.

(94) Nam, J.; Lim, H.; Kim, D.; Jung, H.; Shin, S. Continuous Separation of Microparticles in a Microfluidic Channel via the Elasto-Inertial Effect of Non-Newtonian Fluid. *Lab Chip* **2012**, *12* (7), 1347.

(95) Del Giudice, F.; Romeo, G.; D'Avino, G.; Greco, F.; Netti, P. A.; Maffettone, P. L. Particle Alignment in a Viscoelastic Liquid Flowing in a Square-Shaped Microchannel. *Lab Chip* **2013**, *13* (21), 4263–4271.

(96) Lu, X.; Zhu, L.; Hua, R. mao; Xuan, X. Continuous Sheath-Free Separation of Particles by Shape in Viscoelastic Fluids. *Appl. Phys. Lett.* **2015**, *107* (26).

(97) Xia, Y.; Whitesides, G. M. Soft Lithography. *Angew. Chemie Int. Ed.* **1998**, *37* (5), 550–575.

(98) Schneider, C. A.; Rasband, W. S.; Eliceiri, K. W. NIH Image to ImageJ: 25 Years of Image Analysis. *Nat. Methods* **2012**, *9* (7), 671–675.

(99) Zhang, J.; Yan, S.; Sluyter, R.; Li, W.; Alici, G.; Nguyen, N.-T. Inertial Particle Separation by Differential Equilibrium Positions in a Symmetrical Serpentine Micro-Channel. *Sci. Rep.* **2015**, *4* (1), 4527.